



Geochronology, geochemistry and Sr-Nd isotopes of the granitic rocks associated with tungsten deposits in Beishan district, NW China, Central Asian Orogenic Belt: Petrogenesis, metallogenetic and tectonic implications

Jixin Ding ^{a,b,*}, Chunming Han ^{a,c}, Wenjiao Xiao ^{c,d}, Zhongmei Wang ^a, Dongfang Song ^d

^a Key Laboratory of Mineral Resources, Institute of Geology and Geophysics, Chinese Academy of Sciences, Beijing 100029, China

^b University of Chinese Academy of Sciences, Beijing 100049, China

^c Xinjiang Research Center for Mineral Resources, Urumqi 830011, China

^d State Key Laboratory of Lithospheric Evolution, Institute of Geology and Geophysics, Chinese Academy of Sciences, Beijing 100029, China



ARTICLE INFO

Article history:

Received 30 August 2016

Received in revised form 9 June 2017

Accepted 14 June 2017

Available online 29 June 2017

Keywords:

Tungsten deposits

Granitic rocks

Beishan metallogenetic belt

Central Asian Orogenic Belt

ABSTRACT

The Beishan orogenic belt is an important tectonic unit and a suitable target to investigate and understand the Paleozoic tectonic framework of the Central Asian Orogenic Belt. Paleozoic granitic rocks are widely distributed in the area and closely related to the tungsten deposits at Hongjianbingshan, Guoqing, Yingzuihongshan and Yushan. To understand the petrogenesis of the intrusions, we performed SIMS zircon U-Pb, O and whole rock major-trace element contents and Sr-Nd isotopic analyses. Two major suites of granitic intrusions associated with tungsten mineralization have been recognized during 424–314 Ma and 286–244 Ma. The former suite shows variable Sr-Nd and O compositions (average $(^{87}\text{Sr}/^{86}\text{Sr})_i = 0.7149$ or 0.7034 , $\epsilon\text{Nd}_{(t)} = -6.3$ or 7.6 , $T_{2\text{DM}} = 1.68$ or 0.41 Ga, $\delta^{18}\text{O} = 9.3$ or $5.9\text{\textperthousand}$) indicating an ancient crust or a juvenile lower crust origin, whereas the latter suite shows A-type affinity, and the Sr-Nd and O compositions (average $(^{87}\text{Sr}/^{86}\text{Sr})_i = 0.7125$, $\epsilon\text{Nd}_{(t)} = -4.5$, $T_{2\text{DM}} = 1.42$ Ga, $\delta^{18}\text{O} = 6.9\text{\textperthousand}$) suggest the Precambrian metasedimentary strata may have exerted a significant role in the magma source. The proposed magma sources, combined with the geochemical differences between these two suites of intrusions, indicating the Silurian-Carboniferous mineralization such as Hongjianbingshan, Guoqing and Yingzuihongshan are closely associated with subduction-accretion and generation of Gongpoquan arc-accretionary system, while the Permian mineralization including Yushan deposit are attributed to continuing accretion and subsequent post collision. These tungsten-related granitic rocks are enriched in LREE and depleted in HREE and Ba, Sr, Nb, P, Eu and Ti, suggesting they may have experienced advanced fractional crystallization. Furthermore, a spectacular tetrad effect in their REE distribution patterns has been discovered, showing the granites are highly evolved rocks with strong hydrothermal interaction. The prolonged fractional crystallization and magmatic-hydrothermal interactions have contributed to the formation of the Silurian-Permian tungsten mineralization.

© 2017 Elsevier B.V. All rights reserved.

1. Introduction

The Beishan orogenic belt (BOB) forms a significant part of the Central Asian Orogenic Belt (CAOB) (Fig. 1) (Sengör et al., 1993; Jahn et al., 2004; Windley et al., 2007; Xiao and Kusky, 2009; Xiao et al., 2010; Ao et al., 2012; Song et al., 2013a,b, 2014). During the past fifty years, intensive geological and ore-deposit investigations have led to the recognition of many skarn Cu deposits (e.g.

Huitongshan), porphyry Cu-Mo-Pb deposits (e.g. Gongpoquan, Baishantang and Elegenwulanwula), mafic-ultramafic mineral deposits (e.g. Heishan, Guaishishan and Sidingheishan) and orogenic gold deposits (e.g. Xinjinchang, Laojinchang) (Zuo and He, 1990; Nie et al., 2002a; Yang et al., 2008a, 2009; Zhao et al., 2016) (Figs. 2 and 3; Table 1). However, few tungsten deposits have been focused by now. Although several investigations reported on these deposits and related magmatic suites (Zuo and He, 1990; Zuo et al., 1990; Nie et al., 2002a; Mao, 2008; Xiao et al., 2010), the timing of the magmatic and mineralization events and their geodynamic mechanism still remain controversial (Nie et al., 2004; Jiang and Nie, 2006; Jiang et al., 2006; Ma and Xi, 2012; Yang

* Corresponding author at: No. 19, Beitucheng Western Road, Chaoyang District, Beijing 100029, China.

E-mail address: gelementary@163.com (J. Ding).

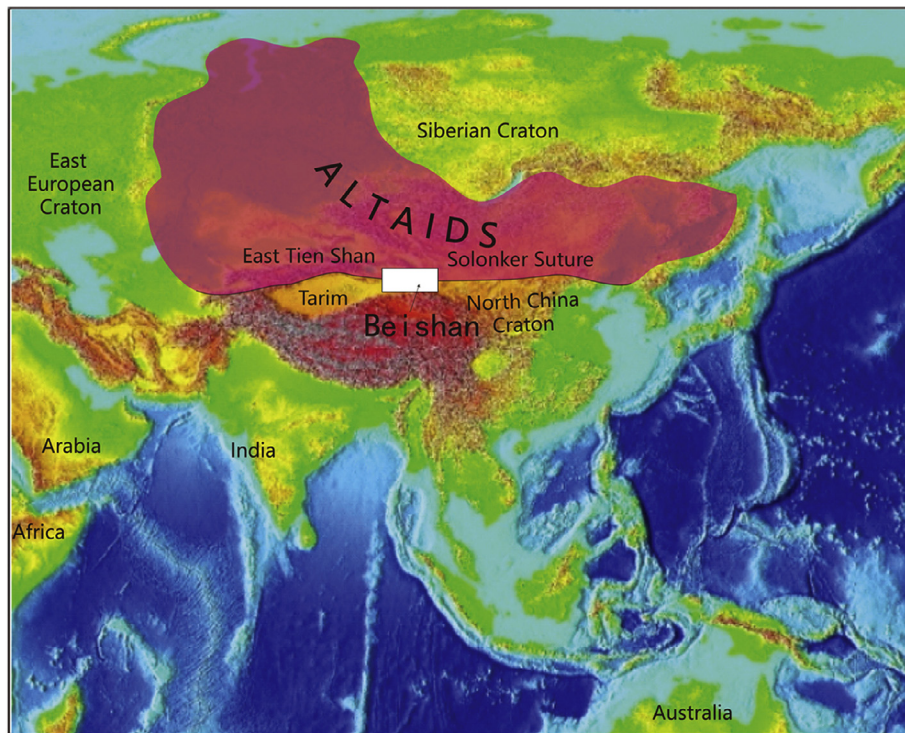


Fig. 1. Digital elevation map showing the key position of the Beishan Orogenic Belt (modified after Xiao et al., 2010). The Altaids or Central Asian Orogenic Belt, composed of orogenic collages between the Siberian, East European, Tarim and North China Cratons, as shown by a transparent reddish color with the Beishan orogenic collage marked by a rectangle.

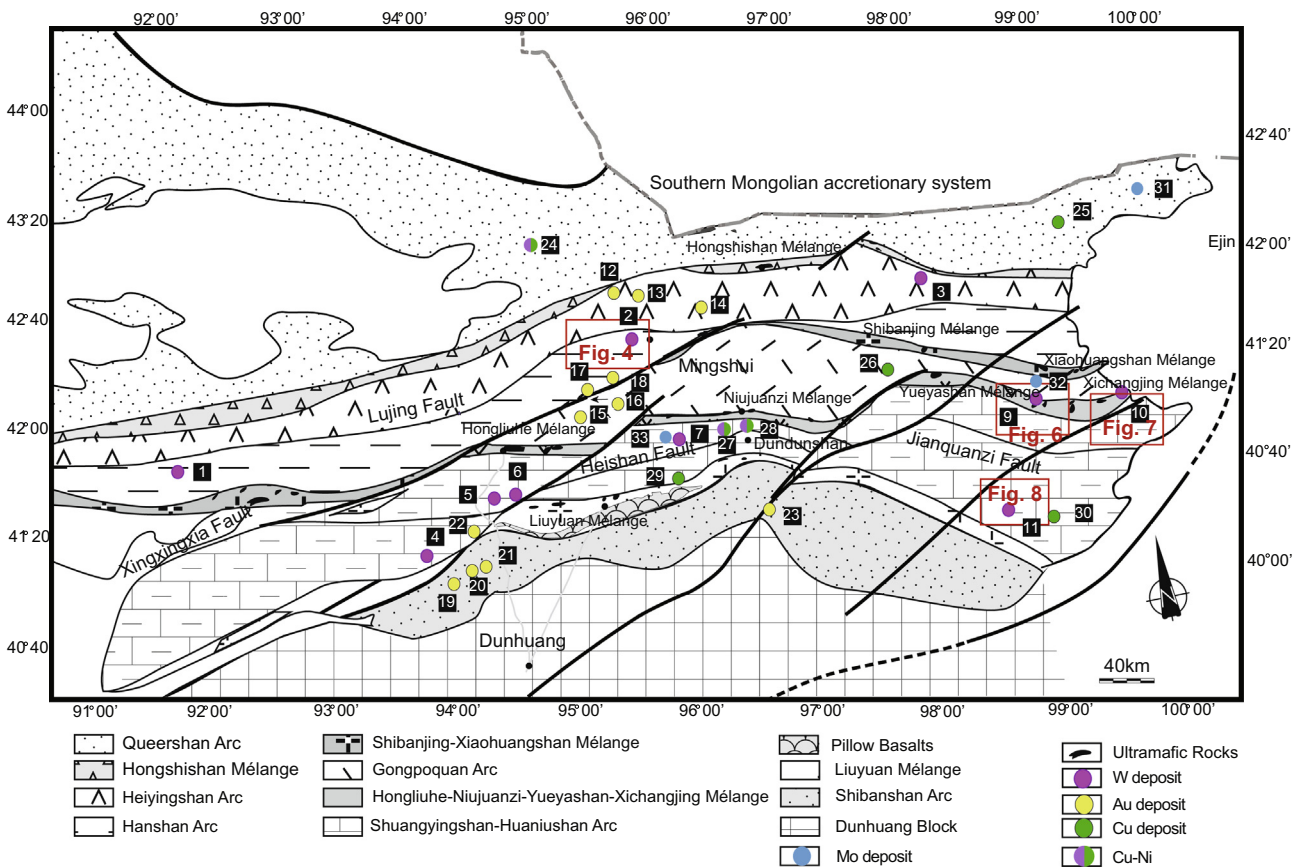


Fig. 2. Simplified tectonic map of the Beishan orogenic collage and its adjacent area showing the tectonic subdivisions (modified after Xiao et al., 2010; Tian et al., 2014).

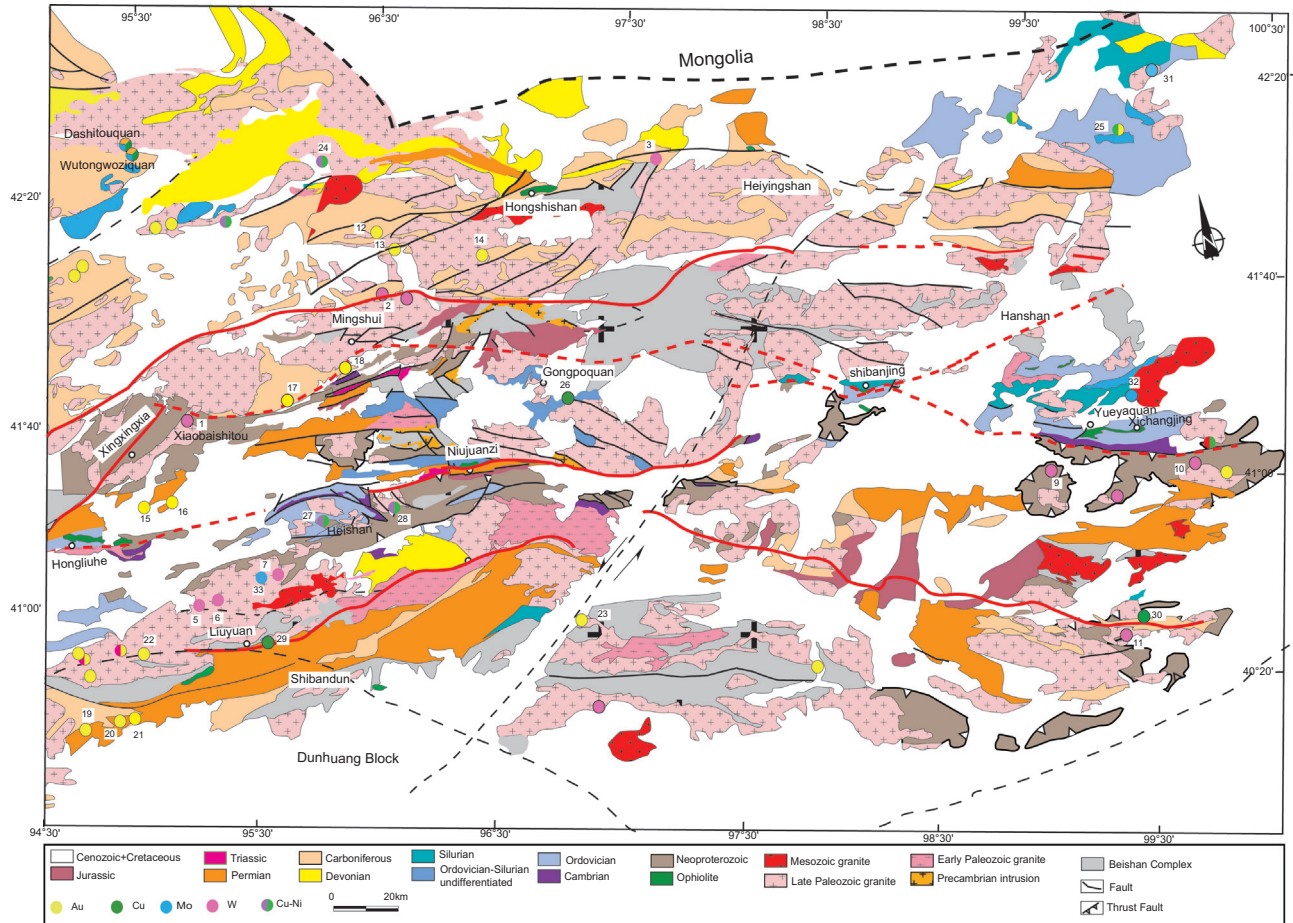


Fig. 3. Geological map of the Beishan orogen, with the Xingxingxia-Hanshan Block and Shuangyingshan-Huaniushan Area marked by bold lines in red, respectively (modified after Song et al., 2013a).

et al., 2008a, 2010; Zhang et al., 2008c; Zhao et al., 2010, 2011, 2012; Ding et al., 2015).

In this paper, we present a comprehensive geochronological and geochemical analysis of the mineralized granitic body from the Beishan metallogenic belt in the southern part of the CAOB, in order to constrain their petrogenesis and geodynamic context and figure out the relationship between the magmatism and mineralization. Our study has significant implications for tungsten exploration in Beishan metallogenic belt and even throughout much of the Central Asia.

2. Geological setting

The BOB contains a number of Paleozoic terranes that accreted between the Siberian and Tarim Craton, and has undergone complex tectonic evolution (Zuo and He, 1990; Zuo et al., 1990, 2003; Nie et al., 2002a; Xiao et al., 2010; Liu et al., 2016). The belt consists of Precambrian overlying metasedimentary rocks, Paleozoic arcs, ophiolitic mélange, accretionary complexes and arc-related basin sediments (Mao, 2008; Tian et al., 2013, 2014; Guo et al., 2012), dividing into five tectonic zones by ophiolitic mélange from north to south: the Queershan arc, the Heiyingshan-Hanshan arc, the Gongpoquan arc, the Shuangyingshan-Huaniushan arc and the Shibanshan arc (Fig. 2), of which the Heiyingshan-Hanshan arc is divided into the Heiyingshan arc and the Hanshan block by the Lujing fault (Fig. 2). The Heiyingshan-Hanshan arc, together with the Gongpoquan arc and the Shuangyingshan-Huaniushan arc constitute the Gongpoquan

arc-accretionary system. Most tungsten deposits are located in this arc-accretionary system.

The amalgamation and evolution of these terranes occurred at various time from Cambrian to Permian and was accompanied by several episodes of magmatism, resulting in large volumes of granitic intrusions and mafic volcanic rocks, accompanied by lesser volumes of mafic-ultramafic intrusions. Most of the magmatism occurred in the Paleozoic time (Zuo and He, 1990; Mao, 2008; Xiao et al., 2010; Han et al., 2016; Su et al., 2013) (Fig. 3). Numerous Hercynian intrusive batholiths and stocks sporadically distributed in the Hanshan block and Huaniushan arc (Jiang, 2004), where the tungsten mineralization were mainly discovered. They are composed of ultramafic rocks, gabbros, quartz diorites, diorites, tonalites, granodiorites, monzonitic granites and K-feldspar granites. Indosinian and Yanshanian granite batholiths and stocks mainly crop out in the eastern and southeastern parts of the BOB (Fig. 3), exhibiting association with the Mo deposits in the study area, including the Qiyishan, Xiaohulishan, Huaniushan and Huahitan. The intrusions were proved to be A-type granites generated in an extensional environment (Zhu et al., 2012). Radiometric dating of these granites indicates that they were emplaced during Permian and Jurassic time (ages range from approximately 290 to 150 Ma; Li et al., 2011; Peng et al., 2010; Yang, 2012; Yang et al., 2008a, 2012; Lv et al., 2011; Zhang et al., 2012b, 2014).

3. Geology of mineral deposits and associated intrusions

In the BOB, there are numbers of granitoid intrusions and related tungsten deposits (Figs. 2 and 3, Table 1). The major ones

Table 1
Basic geologic features of selected tungsten, gold and copper deposits of the metallogenic belt in Beishan domain.

Ore deposits	Longitude/latitude	Genetic types	Host rocks	Oreminerals	Alterations	Grade (g/t), reserve/utility	Main economic elements	References
Xiaobaishitou (1)	95°20'18", 41°53'51"	Skarn	Biotite adamellite	Scheelite, molybdenite	Skarnization, silification, fluoritization, albitionization, carbonatization, chloritization Silification, greisenization	W-Mo	Chen (2006) and Hu et al. (1996)	
Hongjianbingshan (2)	96°22'30", 42°11'44"	Epithermal	Monzogranite	Wolframite, molybdenite, pyrite		1.44% WO ₃	W	Jiang and Nie (2006), Nie et al. (2004), Yang et al. (2008a)
Liushashan (3)	98°23'00", 42°15'16"	Porphyry Au-Mo-(W)	Granodiorite	Wolframite, Au, molybdenite	Silification, sericitization, propylitization		Mo-Au-(W)	Jiang (2004) and Nie et al. (2002b)
Baishandong (4)	93°55'09", 40°52'55"	Epithermal	K-feldspar granite, quartz vein	Scheelite, cassiterite	Greisenization, silification	0.08–0.765% WO ₃	W-(Sn)	Yang et al. (2008a)
Baixianishan (5)	94°50'07", 41°08'24"	Epithermal	Monzogranite	Scheelite, pyrite	Silification, sericitization, fluoritization, carbonatization, propylitization, chloritization	0.076–0.347% WO ₃	W	Sun and Li (2009)
Zhenshifeng (6)	94°53'42", 41°09'00"	Epithermal	Quartz andesite, dacite	Scheelite, molybdenite	Silification, fluoritization, propylitization		W-Mo	Zhou and Sun (2015)
Huanangou (7)	96°26'38", 42°11'20"	Epithermal and porphyry	Granodiorite, monzogranite, K-feldspar granite	Scheelite, molybdenite	Silification, sericitization	0.032% WO ₃	W-Mo	He and Dong (2012)
Guoqing (9)	99°09'10", 41°07'45"	Epithermal	K-feldspar granite, greisen	Wolframite, scheelite	Tourmalinization, greisenization	1.21% WO ₃	W-Sn	Li et al. (2011) and Yang et al. (2008a, 2010)
Yingzuihongshan (10)	99°49'05", 41°05'09"	Epithermal	Monzogranite, biotite mgranite, granite porphyry	Wolframite	Silification, greisenization, tourmalinization, fluoritization	3% WO ₃	W	Yang et al. (2008a, 2010)
Yushan (11)	99°21'45", 40°31'30"	Epithermal	Hongheishan monzogranite, rhyolite	Scheelite	Silification, fluoritization	1.31–2.00% WO ₃	W	Zhang et al. (2008c) and Yang et al. (2008a)
460 (12)	96°22'00", 42°24'35"	Epithermal	Granite porphyry, quartz vein	Chalcopyrite, pyrite, magnetic pyrite, arsenopyrite, native Au	Silification, sericitization, carbonatization, propylitization	7 × 10 ⁻⁶ Au	Au	Yang et al. (2008a)
Saozishan (13)	96°33'42", 42°23'42"	Epithermal	Quartz diorite	Native Au, Ag, pyrite	Propylitization, silification, sericitization, pyritization		Au	He (2015)
Langwashan (14)	97°01'24", 42°14'24"	Epithermal	Hornblende granite, monzogranite	Pyrite, chalcopyrite, magnetite, arsenopyrite, siderite	Silification, sericitization, chloritization, carbonatization		Au	Liu et al. (2009)
Zhaobishan (15)	94°53'25", 41°33'57"	Epithermal	Biotite granite	Native Au, chalcopyrite, pyrite, sphalerite, galena	Silification, sericitization, chloritization		Au	Nie et al. (2002c)
Jinwozi (16)	95°16'41", 41°37'50"	Epithermal	Biotite adamellite, granodiorite	Native Au, Ag, pyrite, galena, stibnite	Beresitization		Au	Zhang et al. (2002) and Wang et al. (2008)
Mazhuangshan (17)	95°49'41", 41°55'33"	Volcanic	Quartz	Native Au, Ag, pyrite, chalcopyrite	Silification, sericitization	7 × 10 ⁻⁶ Au 30 × 10 ⁻⁶ Ag	Au	Yang et al. (2008a) and Jiang (2004)
Nanjinshan (18)	96°08'43", 41°57'43"	Epithermal	Quartz, volcaniclastic rock	Pyrite, sphalerite, galena, arsenopyrite, chalcopyrite, magnetic pyrite, native Au, Ag	Silification, sericitization, carbonatization	7 × 10 ⁻⁶ Au 30 × 10 ⁻⁶ Ag	Au	Jiang (2004) and Yang et al. (2008a)
Shijinpo (19)	95°01'18", 41°10'39"	Epithermal	Monzogranite, granodiorite, quartz vein	Pyrite, sphalerite, galena, native Au	Silification, albitionization, sericitization, carbonatization	5 × 10 ⁻⁶ Au	Au	Hu (2007) and Yang et al. (2008a)
Xinjinchang (20)	94°53'20", 40°55'00"	Volcanic	Granite	Pyrite, sphalerite, galena, arsenopyrite, native Au	Silification, sericitization, chloritization, carbonatization	6 × 10 ⁻⁶ Au 5 × 10 ⁻⁶ Au	Au	Hu (2007), Yang et al. (2008a) and Jiang (2004)
Laojinchang (21)	94°58'20", 40°54'50"	Volcanic	Granite	Pyrite, sphalerite, galena, arsenopyrite, native Au	Silification, sericitization, chloritization, carbonatization	6 × 10 ⁻⁶ Au 5 × 10 ⁻⁶ Au	Au	Hu (2007), Yang et al. (2008a) and Jiang (2004)
Mojindong (22)	95°04'44", 41°10'45"	Epithermal	Porphyritic granite	Native Au, pyrite, galena, chalcocite, native Ag	Silification, sericitization, carbonatization		Au	Jiang et al. (2006)
Xiaoxigong (23)	96°46'34", 40°49'37"	Epithermal	Dacite, K-feldspar granite, granite porphyry	Pyrite, sphalerite, galena, arsenopyrite, chalcopyrite, magnetic pyrite, native Au, Ag	Silification, sericitization, chloritization, carbonatization	3 × 10 ⁻⁶ Au	Au	Jiang (2004), Hu (2007) and Yang et al. (2008a)
Sidingheishan (24)	96°07'30", 42°37'30"	Magmatic deposits	Mafic-supermafic rocks	Pyrrhotite, pentlandite, chalcopyrite, pyrite	Sphalerite, talcization, chalcocite		Cu-Ni	Dai (2010)

Table 1 (continued)

Ore deposits	Longitude/latitude	Genetic types	Host rocks	Oreminerals	Alterations	Grade (g/t), reserve/utility	Main economic elements	References
Elegewulawula	99°02'24'', 42°22'20'' (25)	Porphyry copper deposit	Tonalite-porphyry	Pyrite, chalcopyrite	Greisenization, sericitization, chloritization, pyritization	0.69% Cu	Cu	Liu et al. (2001)
Gongpoquan (26)	97°14'00'', 41°44'11''	Porphyry copper deposits	Granodiorite porphyry, quartz diorite porphyry, dacite	Chalcopyrite, pyrite, pyrrhotite, arsenopyrite, sphalerite, galena	Potassic, silicification, chloritization, propylitization	0.12%Cu, 0.33% Ni	Cu	Xu et al. (2010) and Yang et al. (2008a)
Heishan (27)	95°59'58'', 41°23'03''	Magmatic deposits	Pyroxenite, gabbro	Pyrrhotite, pentlandite, chalcopyrite, pyrite	Serpentinitization, chloritization	0.12%Cu, 0.33% Ni	Cu-Ni	Yang et al. (2008a)
Guaijishan (28)	96°09'30'', 41°26'30''	Magmatic deposits	Mafic-supernafic rocks	Pyrrhotite, pentlandite, chalcopyrite, pyrite	Sphalerite, talcization, chalcocite	0.12%Cu, 0.33% Ni	Cu-Ni	Yang et al. (2016)
Huitongshan (29)	95°14'10'', 41°05'47''	Skarn	K-feldspar, skarn	Chalcocite, chalcopyrite, pyrite, sphalerite	Skarnization, epidotization	1.2% Cu	Cu	Yang et al. (2008a)
Baishantang (30)	99°27'00'', 40°38'05''	Porphyry copper deposit	Rhyodacitic porphyry, tuff lava	Pyrite, chalcopyrite, pyrrhotite, galena, sphalerite	Potassic, silicification, chloritization, propylitization	1.07%Cu, 2.0%Pb	Cu-Pb	Hui et al. (2013), Yang et al. (2008a), You (2002) and Cheng and Zhang (2012)
Xiaohulishan (31)	101°13'20'', 42°25'37''	Porphyry Molybdenum deposit	Granite porphyry	Molybdenite, pyrite, sphalerite, galena, magnetite	Silicification, pyritization	Mo	Mo	Peng et al. (2010), Yang et al. (2012) and Yang (2012)
Qiyishan (32)	99°35'51'', 41°23'01''	Epithermal	Alkali-feldspar granite	Molybdenite, wolframite, cassiterite	Fluoritization, greisenization, skarnization, albitization, chloritization	0.17% WO ₃ , 0.28% Sn, 0.133% Rb, 0.052% Mo, 0.172% Be	Rb-Mo-(W-Sn)e	Lv et al. (2011) and Zhang et al. (2014)
Huanishan (33)	95°33'50'', 41°13'49''	Epithermal	K-feldspar granite	Molybdenite, scheelite	Silicification,	Mo-(W)	Zhu et al. (2012)	

are represented by the Hongjianbingshan (Hjbs), Guoqing (GQ), Yingzuihongshan (YZHS) and Yushan (YS), of which the GQ, YZHS and YS are located in the Shuangyingshan-Huanishan arc, whereas the Hjbs is situated in the Hanshan terrane (Fig. 2).

3.1. Hjbs deposit

The Hjbs deposit is situated in the western part of Hanshan terrane, immediately adjacent to the southern part of the EW-trending Lujing fault (Fig. 2). The tungsten mineralization primarily occurred as topaz-quartz veins within the Hjbs monzogranite stocks (Appendix Fig. 1 b, c), and occasionally as massive blocks within the greisen and albitization monzogranite (Fig. 4), with inferred average WO₃ grades of 1.55 wt% and 0.40 wt%, respectively. Furthermore, both the greisens (Appendix Fig. 1a) and albitization monzogranite were formed by magmatic hydrothermal alteration of the monzogranite during mineralization. The boreholes information have also revealed the mineralization is mainly and closely associated with the monzogranite magmatism.

The Hjbs monzogranite intrudes into the rhyolite tuff. The rock is distributed in the western part of the mine and orients in a SW-NE direction with an exposed area of 5 km² (Fig. 4). The medium-to fine-grained massive pluton is composed of quartz (20–30 vol. %), K-feldspar (30 vol.%), plagioclase (25–40 vol.%) and biotite (5–10 vol.%) (Fig. 5g), as well as accessory minerals including topaz, zircon, sphene, magnetite and pyrite. The rhyolite tuff is gray and shows rhyolitic structure, with feldspar/quartz phenocrysts ranging from 0.5 to 1 mm (occasionally up to 2 mm) in length (15–40 vol.%) (Fig. 5h), the microcrystals mainly consist of felsic components, with accessory minerals including muscovite, biotite and opaque Fe-Ti oxides.

Individual tungsten bodies can be traced along strike for 120–420 m, and down dip for 800–1200 m, with thickness ranging from 0.19 to 132 m. EW- and NE-trending faults and fractures are well developed, and are considered as the main controlling factors of mineralization. Ore minerals mainly include wolframite, cassiterite, molybdenite, bismuthinite, galena, sphalerite, scheelite, chalcopyrite, pyrite and magnetite. Gangue minerals consist of quartz, topaz, helvine, K-feldspar, albite, muscovite, sercite, fluorite and calcite. Alterations related to tungsten mineralization consist mainly of greisenization, silicification, albitization, sericitization, K-feldspathization, epidotization and skarnization (Li, 2011a).

3.2. GQ deposit

The GQ deposit is located at eastern part of Shuangyingshan-Huanishan terrane, 15 km south of Yueyaquan-Xichangjing mélange with an outcrop area of 5 km² (Fig. 2). The deposit has inferred resources of 20,000 tonnes of 1.21 wt% WO₃ (Yang et al., 2010).

Two pulses of intrusions have been identified in the GQ pluton. The earlier granodiorite exposed in the south, comprising about 10% of the outcrop area of the pluton, while the later GQ K-feldspar granite located in the north and mineralized with tungsten, accounting for about 90% of the pluton. The GQ K-feldspar granite is oriented and elongated in an EW direction which intrudes into the Mesoproterozoic Gutongjing metamorphic rocks (Zhao et al., 2012) and is covered by the Quaternary sediments (Fig. 6). The coarse- to medium-grained Guoqing K-feldspar granite composed of quartz (30–50 vol.%), muscovite (10–30 vol.%), plagioclase (20–35 vol.%), microcline (~15 vol.%) (Fig. 5a, b) and tourmaline (~5 vol.%), with accessory minerals including magnetite, zoisite, ilmenite, sercite, sphene and apatite. Parts of the microcline, plagioclase and biotite have been replaced by flaky muscovite or sercite (Fig. 5a, b).

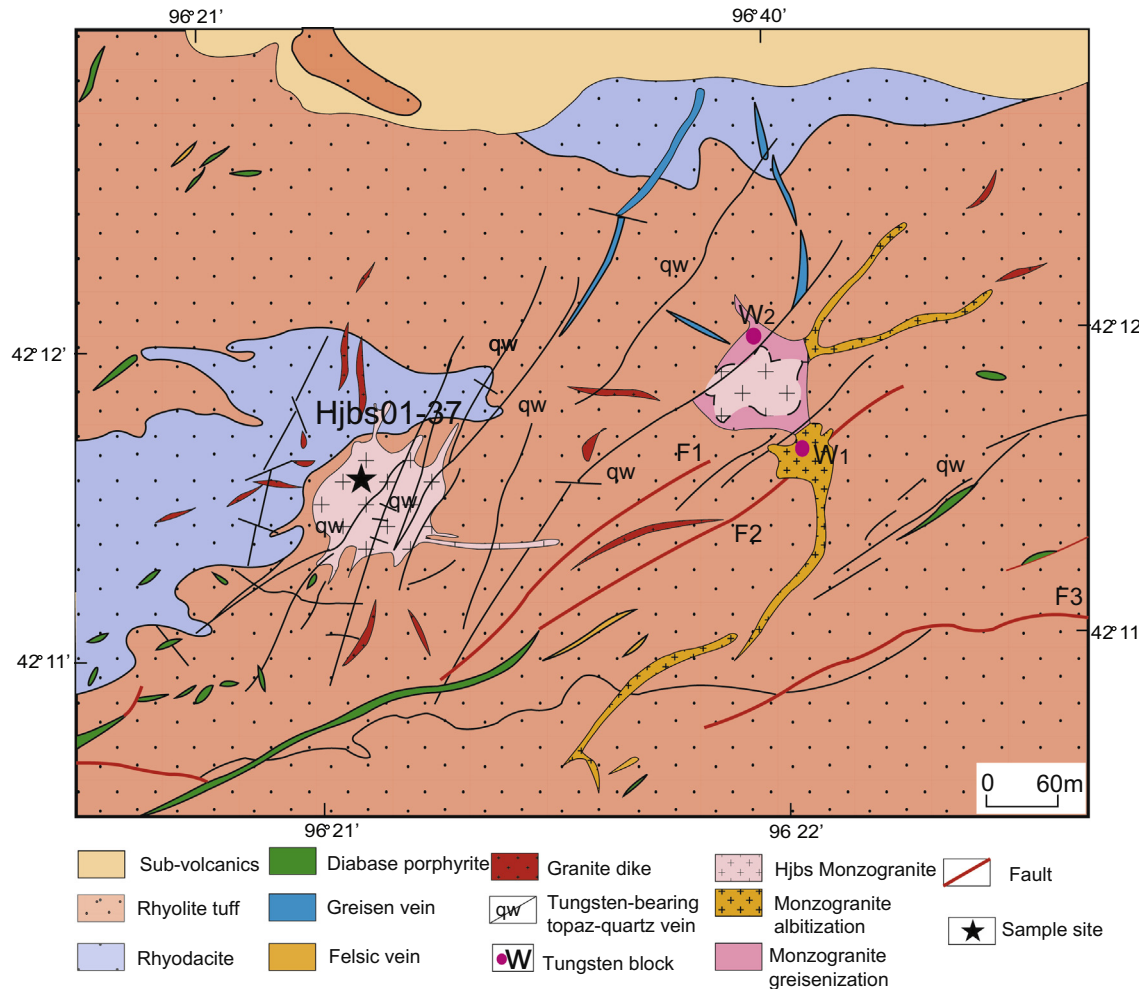


Fig. 4. Geological map of Hongjianbingshan tungsten deposit.

Tungsten mineralization primarily exists within the GQ K-feldspar granite. Quartz-vein- and greisen-type wolframite ore are presented at the deposit. The quartz-vein-type ores are hosted in the K-feldspar granites (Appendix Fig. 1 d) distributed locally along the contact between K-feldspar granites and metasedimentary rocks of the Mesoproterozoic Gutongjing Group (Fig. 6). These ore bodies are 15–225 m long, and 0.5 to 11 m wide, with declined depth of 20–258 m. Most of these ore bodies strike NE, NW and EW. The massive greisen-type ores occur in greisen or altered K-feldspar granite stocks as blocks and stratoid layers. The ores are composed of wolframite, molybdenite, chalcopyrite and pyrite. Gangue minerals consist of quartz, tourmaline, muscovite and sericite. Alterations related to tungsten mineralization consist mainly of tourmalinization, silicification and greisenization.

3.3. YZHS deposit

The YZHS deposit is located 80 km east of the GQ deposit (Figs. 2 and 3), with an outcrop of 150 km² and an average WO₃ grade of 3.00 wt% (Yang et al., 2010).

Many felsic dikes and offshoots which intrude into the Mesoproterozoic Pingtoushan Group metasedimentary rocks are scattered throughout the YZHS area. Petrologically, an early porphyritic monzogranite unit and a late biotite granite unit have been recognized (Fig. 7). There are also small amounts of granite porphyries. The contacts between different petrographic phases

are sharp but no chilled margin has been observed. The YZHS monzogranite exhibits porphyritic texture and consists of quartz (~50 vol.%), plagioclase (~10 vol.%), perthite (~20 vol.%) and biotite (~10 vol.%), as well as accessory minerals including magnetite, zircon and tourmaline (Fig. 5c, d). Most of the monzogranites are subjected to weak silification and greisenization alteration near the contact zones with the Mesoproterozoic strata, and they carry minor disseminated wolframite, pyrite and molybdenite. The foregoing geological evidences indicate that the monzogranites are temporally and spatially associated with the mineralization (Appendix Fig. 1e, f). The biotite granite outcrops as two small intrusions in the YZHS deposit area (Fig. 7), the coarse- to medium-grained intrusions are pink in color and show typical granitic texture. However, a direct contact between these biotite granites and the orebodies has not been observed in the YZHS deposit area. The younger granite porphyry is emplaced along the scattered fractures developed in YZHS monzogranite.

The YZHS deposit is 1800 m in length and up to 800 m in width, with a thickness of 70–140 m. The ores are primarily quartz-vein-type, characterized by disseminated and vein structures. Principal ore minerals are wolframite and scheelite with minor quantities of chalcopyrite, pyrite, molybdenite, galena and arsenopyrite. The gangue minerals include tourmaline, K-feldspar, sericite, beryl, topaz, fluorite and calcite. Alterations related to tungsten mineralization consist mainly of tourmalinization, silicification, greisenization, sericitization and pyritization.

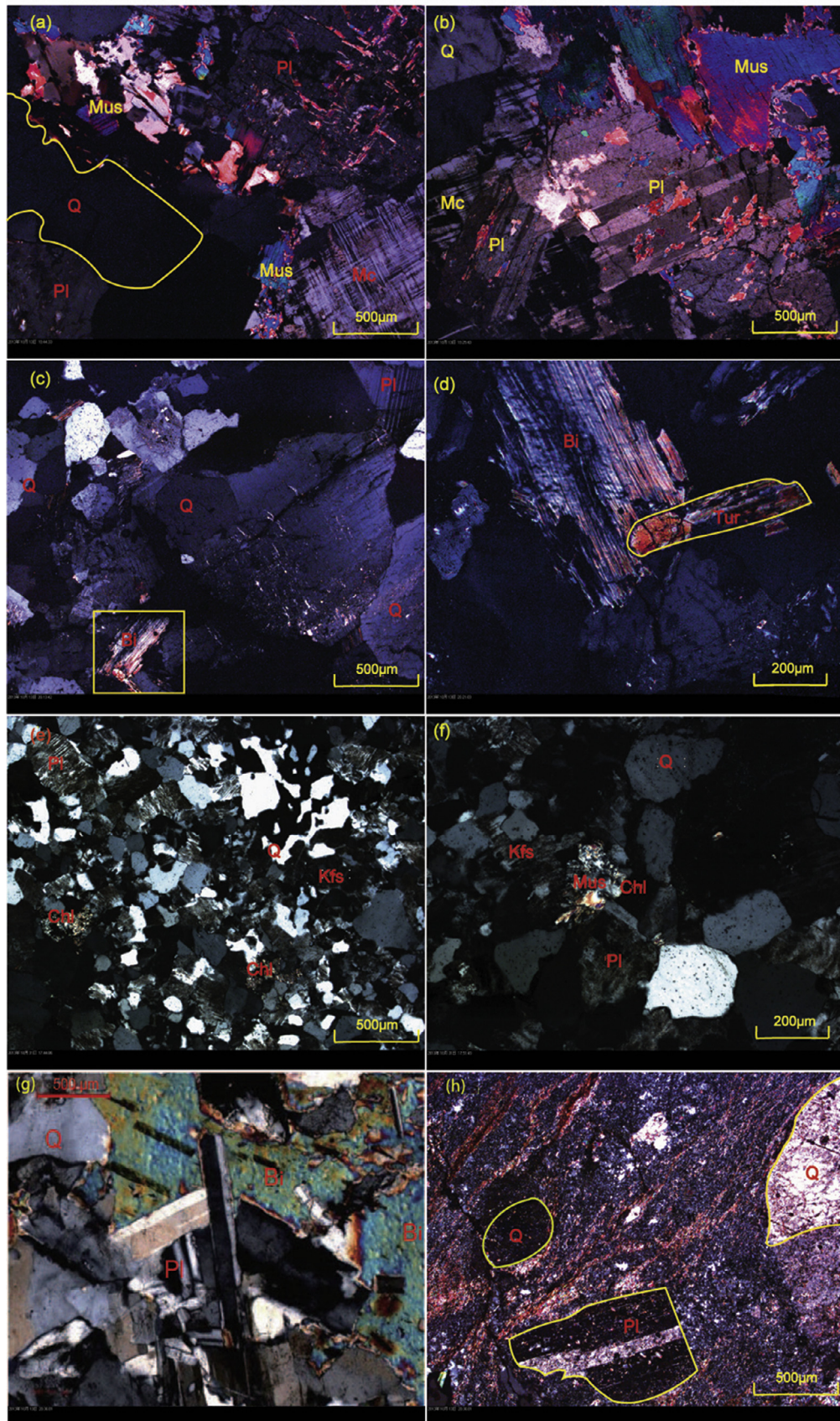


Fig. 5. Photomicrographs of rocks associated with tungsten mineralization in the BOB. K-feldspar granite (a, b) from GQ deposit (sample GQ01-21, GQ02-17 respectively); Quartz, plagioclase, biotite in the monzogranite (c) and tourmaline in monzogranite (d) from YZHS deposit (sample YZHS02-21); Quartz, K-feldspar and plagioclase in the granite (e, f) from YS deposit, with feldspar replaced by chlorite and muscovite (sample YS03-11); monzogranite (g) and rhyolite tuff from Hjbs deposit (sample Hjbs01-37 for monzogranite). Mineral abbreviations: Q – quartz; Pl – plagioclase; Mus – muscovite; Bi – biotite; Tur – tourmaline; Mc – microcline; Chl – chlorite; Kfs – K-feldspar.

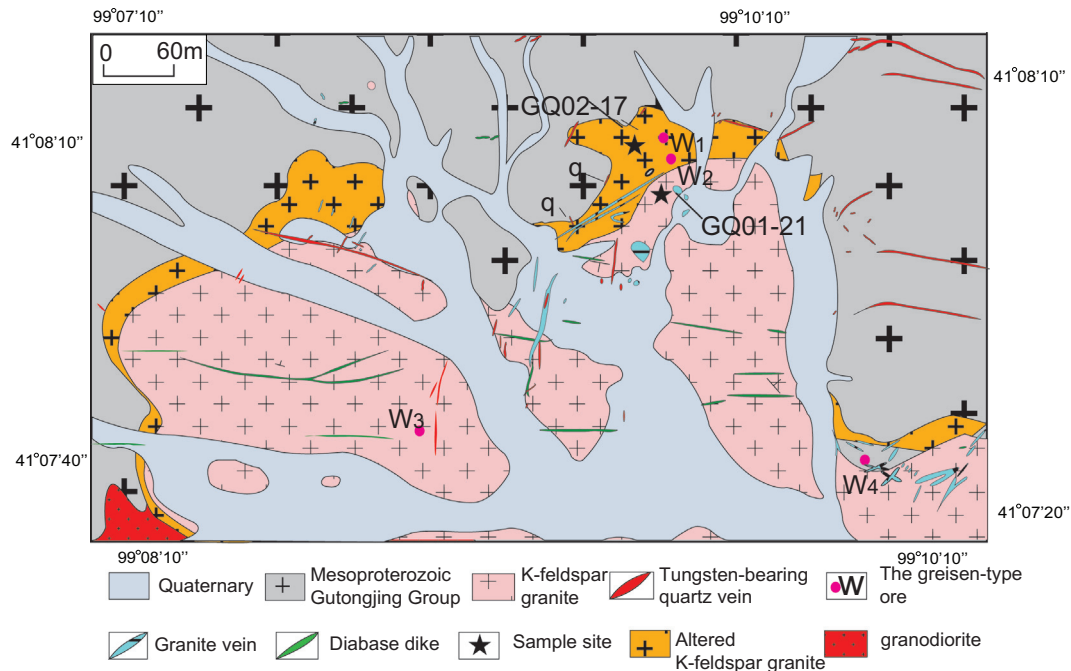


Fig. 6. Geological map of Guoqing tungsten deposit.

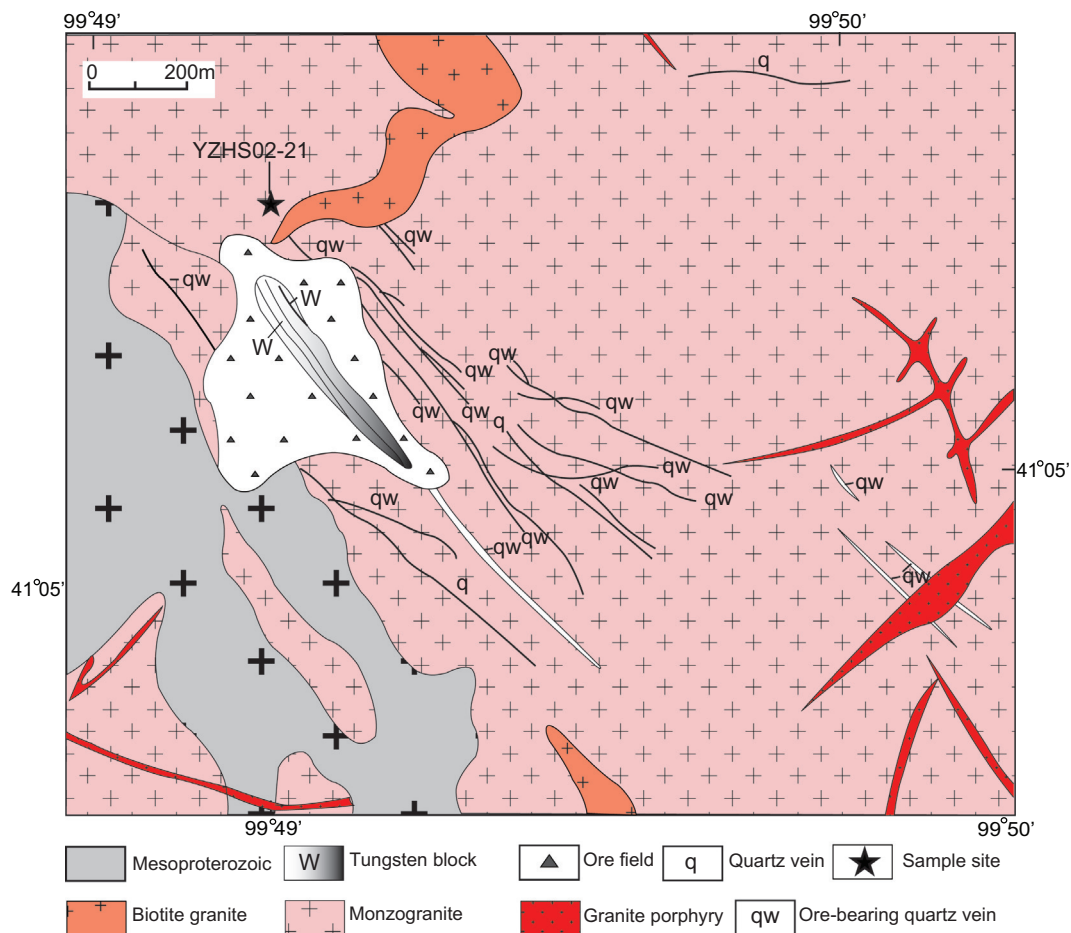


Fig. 7. Geological map of Yingzuihongshan tungsten deposit.

3.4. YS deposit

The YS deposit lies in the south of the Huaniushan terrane (Fig. 2). Exploration work indicates that the YS contains 15,000 tonnes WO_3 , with ore grades of 1.31–2.00 wt%.

The YS pluton intrudes into the Mesoproterozoic Pingtoushan Formation, the Lower Carboniferous limestone, marble and volcanics with a total exposed area of 100 km². The pluton composed mainly of the Hongjishan monzogranite and the Hongheishan K-feldspar granite (Fig. 8). The Hongjishan monzogranite accounts for 50% of the pluton and distributes in the western part. The Hongheishan K-feldspar granite (i.e. YS K-feldspar granite) make up about 40% of the outcrop area in the eastern part and is strongly mineralized (Appendix Fig. 1 g, h). The YS K-feldspar granite has a typical medium- to fine-grained granitic texture, consisting of quartz (~40 vol.%), K-feldspar (~40 vol.%), plagioclase (<10 vol.%) and a small amount of mafic minerals (biotite and amphibole) (Fig. 5e), with accessory minerals comprising zircon, apatite, ilmenite and fluorite. Parts of the K-feldspar are replaced by chlorite and muscovite (Fig. 5f).

The deposit is 1400 m long and up to 135 m wide. Three groups of faults with WNW-, NE- and NNE-trending strikes are observed. The WNW-trending faults are large-scale, and have undergone multiple stages of movement. Quartz-vein-type ores are discovered at YS, occur as lens (Appendix Fig. 1 h) and veins and veinlets. Ore minerals are dominantly scheelite, magnetite, hematite and limonite. Gangue mineral are mainly calcite, quartz and fluorite. Four mineralization stages can be identified (Zhang et al., 2008c): (1) diopside-vesuvianite-wollastonite; (2) fluorite-scheelite; (3) fluorite-scheelite-pyrite-chalcopyrite; (4) pyrite-chalcopyrite-calcite.

4. Sampling and analytical methods

A total of 200 granitoid samples were collected from the Hjbs monzogranite (Hjbs01-), GQ K-feldspar granite (GQ01-, GQ02-), YZHS monzogranite (YZHS02-) and YS K-feldspar granite (YS03-), both spread along the W-(Sn/Mo) related central granitoid belt. 58 samples were selected for geochemical analysis, 36 for Rb-Sr and Sm-Nd analysis. Zircon U-Pb dating and O-in-zircon isotope analysis were performed on five samples named Hjbs01-37, GQ01-21, GQ02-17, YZHS02-21 and YS03-11, with the thin sections prepared for petrographical and mineralogical investigations. The sample locations are shown in chapter 5.1.

4.1. SIMS zircon U-Pb dating and O isotope analysis

Zircons were separated from five granite samples using heavy liquid and magnetic separation technique and then handpicked under a binocular microscope. The grains were mounted on adhesive tape, enclosed in epoxy resin and polished to approximately half their thickness. To observe the internal structure and select a potential target site for U-Pb and O isotopic analyses, cathodoluminescence (CL) imaging was conducted using a JXA8100 electron microprobe for high-resolution imaging spectroscopy at the Institute of Geology and Geophysics, Chinese Academy of Sciences (IGGCAS), Beijing.

4.1.1. SIMS zircon U-Pb dating

Zircon U-Pb isotopes were analyzed on a Cameca 1280 SIMS at the IGGCAS, Beijing. U-Pb ratios were determined relative to the standard zircon Plešovice (Sláma et al., 2008), and the absolute abundances of the test were determined relative to the standard

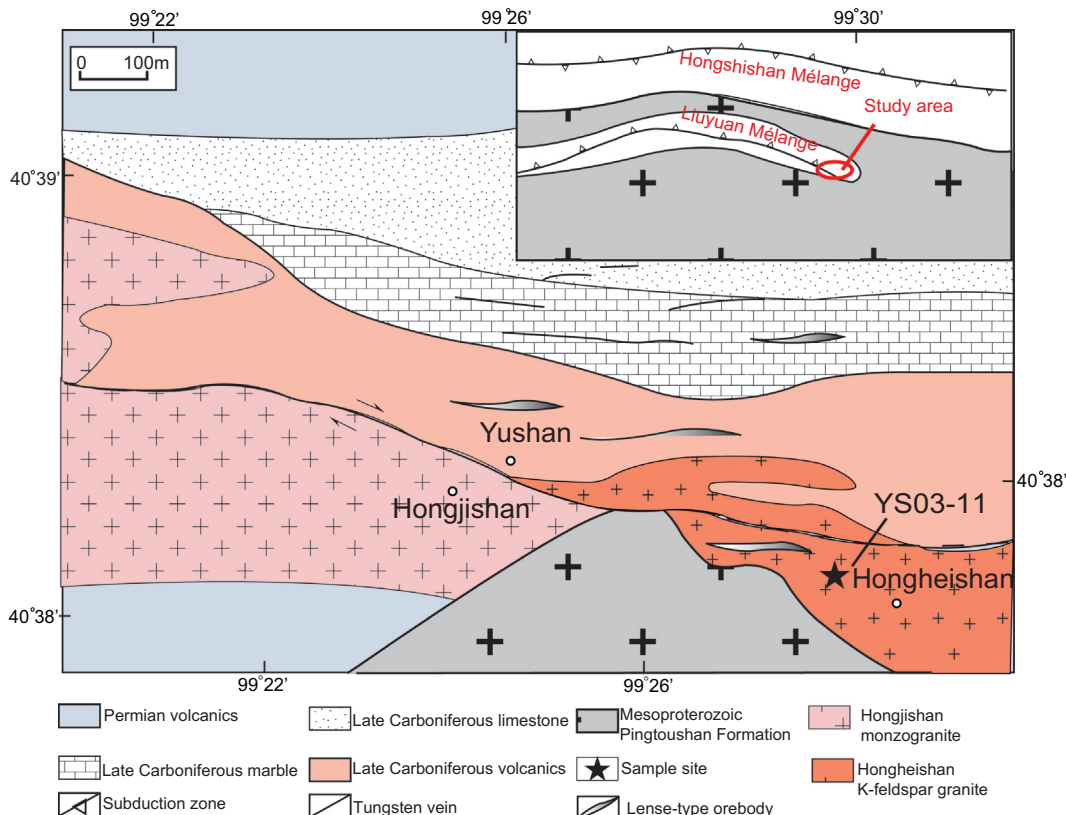


Fig. 8. Geological map of Yushan tungsten deposit.

zircon M257 (Nasdal et al., 2008). For the detailed test flow and data-processing method, see Li et al. (2009). Measured ^{204}Pb value was used for correction of common Pb content. Because the common Pb content was very low, an average Pb of present-day crustal composition (Stacey and Kramers, 1975) is used for the common Pb correction assuming that it is largely due to surface contamination introduced during sample preparation. Uncertainties on individual analysis in the data table are reported at 1σ level, mean ages for pooled U/Pb analyses are quoted with 95% confidence intervals. Data reduction was carried out using the Isoplot/Exev. 2.49 program (Ludwig, 2003).

4.1.2. SIMS zircon oxygen isotopes

Zircon oxygen isotopes were conducted on the same grains as those analyzed for U-Pb dating on the same Cameca 1280 SIMS. The Cs^+ ion beam was accelerated to 10 kV, with an intensity of $\sim 2\text{nA}$. Analytical procedures are as same as those described by

Li et al. (2010a). The instrumental mass fractionation factor (IMF) was corrected using Penglai zircon standard with $\delta^{18}\text{O}$ value of 5.31‰ (Li et al., 2010b). The internal precision of a single analysis was generally better than 0.20‰ (1σ standard error) for $^{18}\text{O}/^{16}\text{O}$ ratio. The external precision, measured by the reproducibility of repeated analyses of Penglai standard during two sections of this study, is 0.43‰ (2SD, $n = 13$) and 0.34‰ (2SD, $n = 17$).

4.2. Major and trace elements analysis

58 samples were crushed into granules less than two hundred mesh and then analyzed for major and trace elements. All of the analyses were carried out at the State Key Laboratory of Lithospheric Evolution, IGGCAS, Beijing. Major oxides were determined by X-ray fluorescence (XRF) spectrometry using a Shimadzu XRF1500 sequential spectrometer, with analytical uncertainties ranging from 1% to 5%. Trace-element abundances were measured

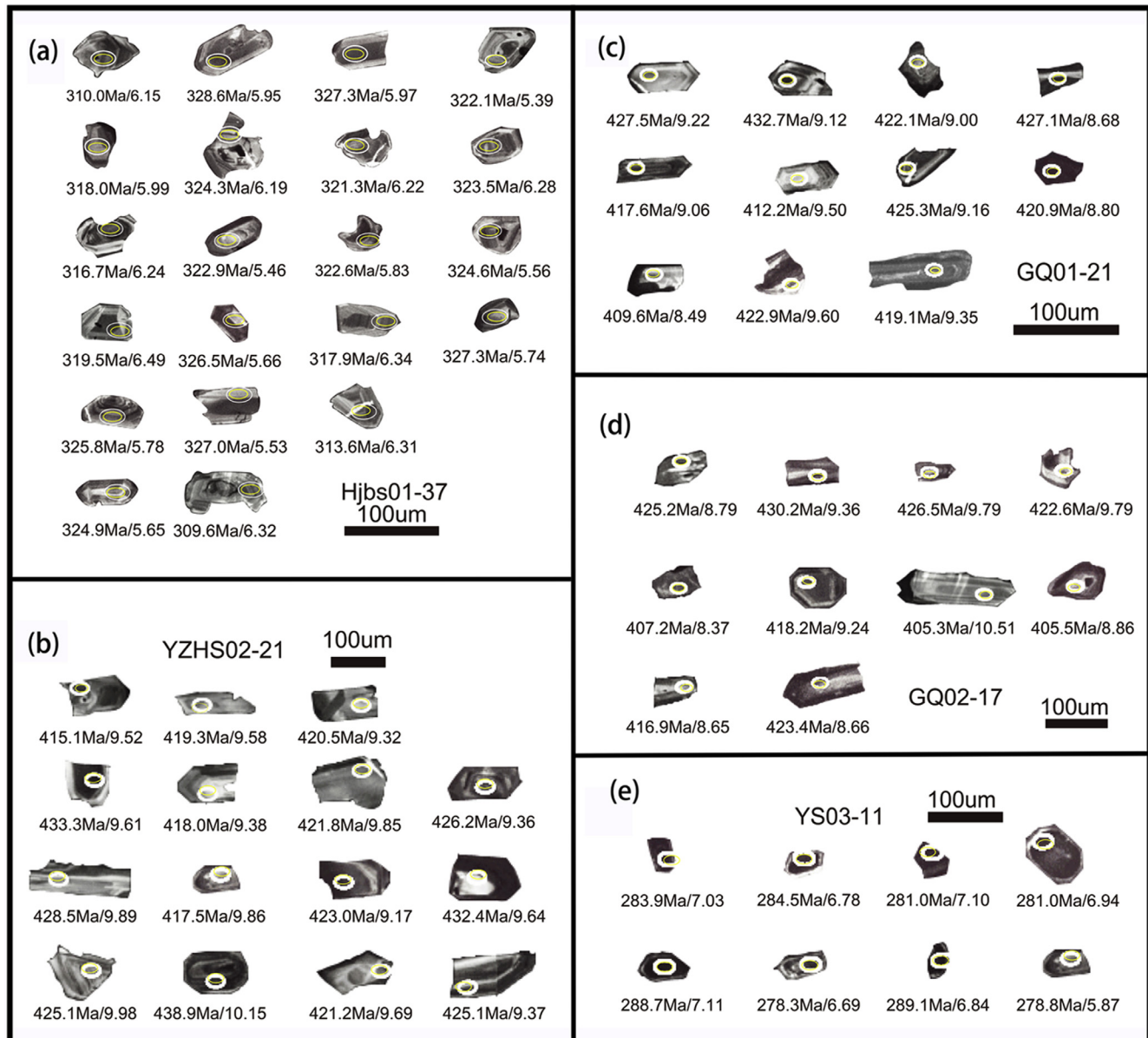


Fig. 9. Cathodoluminescence (CL) images of representative zircon grains for the granites. The white and yellow circles indicate the analytical areas for SIMS U-Pb dating and O-isotope. Numerals in white color below the circles indicate U-Pb age (Ma) and $\delta^{18}\text{O}$ (‰) values, respectively.

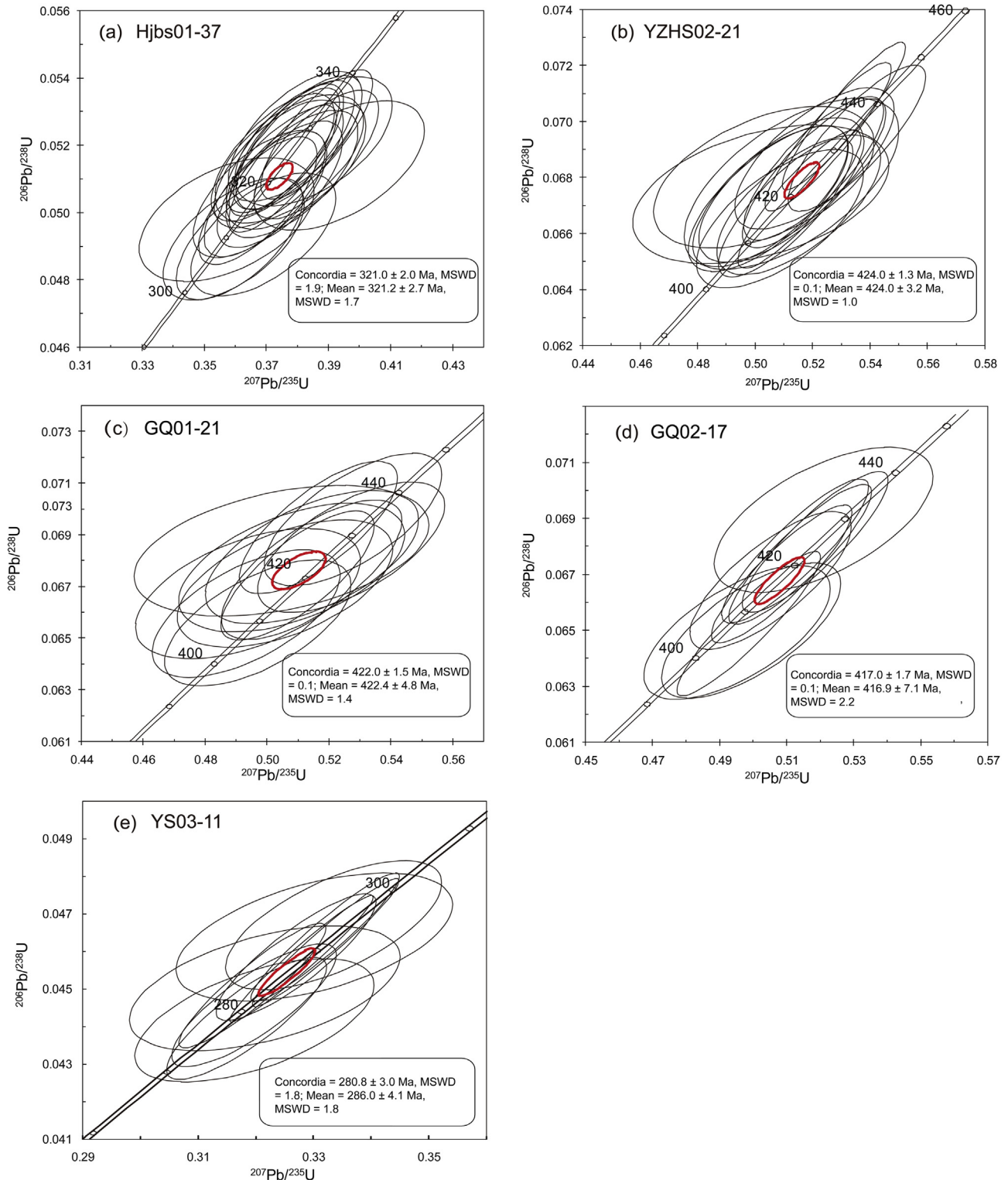


Fig. 10. Zircon U-Pb concordant diagrams from the granites in Beishan Orogenic Belt.

by Inductively Coupled Plasma Mass Spectrometry (ICP-MS) using a Finnigan MAT Element spectrometer, further detailed description of the procedures is provided by Gao et al. (2002). According to Chinese national standards GSR-1 and GSR-2, the error was <5% for trace elements with concentrations >10 ppm and <10% for trace elements with concentrations <10 ppm. Major and trace element analyses are listed in Appendix Table 3.

4.3. Rb-Sr, Sm-Nd isotope analysis

Rb-Sr and Sm-Nd isotopes were separated using conventional ion exchange procedures and measured using a Finnigan MAT 262 multi-collector mass spectrometer at IGGCAS, Beijing. The measurement were carried out following the isotope dilution procedures of Yang et al. (2006). Procedural blanks were <100 pg for

Sm and Nd and <500 pg for Rb and Sr. $^{143}\text{Nd}/^{144}\text{Nd}$ were corrected for mass fractionation by normalization to $^{146}\text{Nd}/^{144}\text{Nd} = 0.7219$ and $^{87}\text{Sr}/^{86}\text{Sr}$ ratios normalized to $^{86}\text{Sr}/^{88}\text{Sr} = 0.1194$. Typical within-run precision (2σ) for Sr and Nd was estimated to be ± 0.000015 . The measured values for the La Jolla and BCR-1 Nd standards and the NBS-607 Sr standard were $^{143}\text{Nd}/^{144}\text{Nd} = 0.511853 \pm 7$ ($2\sigma_n$, $n = 3$) and 0.512604 ± 7 ($2\sigma_n$, $n = 3$) and $^{87}\text{Sr}/^{86}\text{Sr} = 1.20042 \pm 2$ ($2\sigma_n$, $n = 12$) during the period of data acquisition.

5. Results

5.1. Zircon U-Pb geochronology

The CL images for the dated zircons from Hjbs, YZHS, GQ and YS granite are presented in Fig. 9 and the U-Pb age data are listed in Appendix Table 1 and shown in Fig. 10.

Twenty-two analyses from sample Hjbs01-37 ($96^{\circ}21'11.3''\text{E}$, $42^{\circ}11'44.5''\text{N}$) were obtained. Zircons from the monzogranite generally display well-preserved concentric oscillatory zoning (Fig. 9a). The uranium concentrations range from 110 to 559 ppm, thorium from 202 to 670 ppm, and the Th/U ratios are relatively high (0.47–0.86) (Appendix Table 1), indicating a magmatic origin (Hoskin and Black, 2000). The analyses yield excellent concordant results with a weighted mean $^{206}\text{Pb}/^{238}\text{U}$ age of 321.2 ± 2.7 Ma (MSWD = 1.7) (Fig. 10a), which is interpreted as the crystallization age of the monzogranite at Hjbs.

Fifteen analyses from sample YZHS02-21 ($99^{\circ}49'14.2''\text{E}$, $41^{\circ}05'13.4''\text{N}$) were obtained. Zircons from the monzogranite are mostly euhedral, and colourless. In CL images (Fig. 9b), no inherited cores were observed. Zircons have high uranium (from 56 to 490 ppm) and Th (from 145 to 1021 ppm) contents, and high Th/U ratios (from 0.31 to 0.75, mostly > 0.4) (Appendix Table 1). Such features indicate that they were crystallized from magmas. The analyses form a tight cluster on Concordia and yield a weighted mean $^{206}\text{Pb}/^{238}\text{U}$ age of 424.0 ± 3.2 Ma (MSWD = 1.0) (Fig. 10b), which we consider to be the best estimate of the crystallization age of the monzogranites at YZHS.

Zircons in the K-feldspar granites from GQ deposit (GQ01-21, GQ02-17) are mainly euhedral, prismatic, and colourless, with oscillatory zoning, indicating a magmatic origin (Fig. 9c, d). Eleven analyses from sample GQ01-21 ($99^{\circ}09'35.4''\text{E}$, $41^{\circ}07'55.9''\text{N}$), were obtained. The uranium concentrations range from 117 to 939 ppm, thorium from 152 to 1944 ppm, and the Th/U ratios are relatively high (0.16–0.55) (Appendix Table 1). All the 11 analyzed zircons yield excellent concordant results with a weighted mean $^{206}\text{Pb}/^{238}\text{U}$ age of 422.4 ± 4.8 Ma (MSWD = 1.4) (Fig. 10c). Ten analyses from sample GQ02-17 ($99^{\circ}09'35.8''\text{E}$, $41^{\circ}07'57.1''\text{N}$) were obtained. The uranium concentrations range from 17 to 243 ppm, thorium from 188 to 970 ppm, and the Th/U ratios are relatively high (0.02–0.47) (Appendix Table 1). All the 10 analyzed zircons yield excellent concordant results with a weighted mean $^{206}\text{Pb}/^{238}\text{U}$ age of 416.9 ± 7.1 Ma (MSWD = 2.2) (Fig. 10d). We consider the crystallization age of the K-feldspar granites at the GQ deposit (417–422 Ma) to be the best estimation from the current data described above.

Eight analyses from sample YS03-11 ($99^{\circ}27'12.9''\text{E}$, $40^{\circ}37'50.5''\text{N}$) were obtained. Zircons from the K-feldspar granite are mostly small, euhedral and colourless (Fig. 9e). Zircons have high uranium (505–2326 ppm) and Th (1087–3709 ppm) contents, and high Th/U ratios (0.47–1.15) (Appendix Table 1). Eight analyses form a tight cluster on the Concordia diagram, yielding a weighted mean $^{206}\text{Pb}/^{238}\text{U}$ age of 286.0 ± 4.1 Ma (MSWD = 1.8) (Fig. 10e), which is considered to be the best estimate of the crystallization age of the K-feldspar granites at YS deposit.

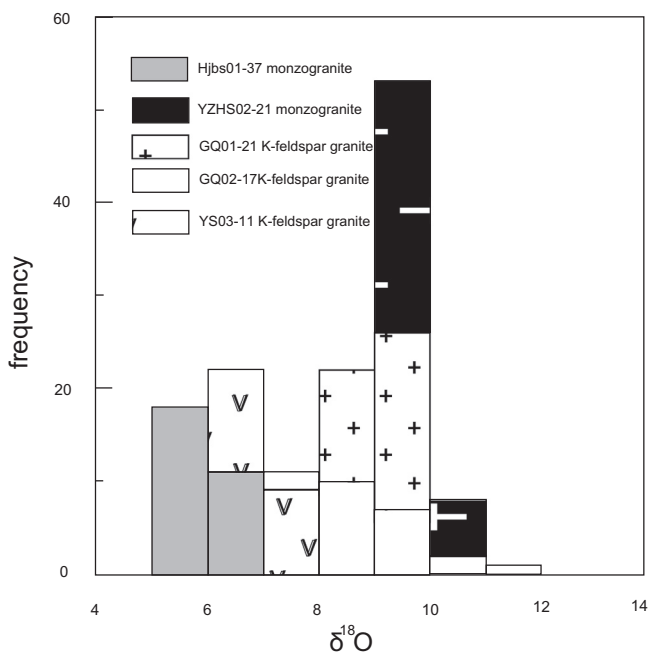


Fig. 11. Probabilistic histogram of $\delta^{18}\text{O}$ values for the ore-bearing rocks.

5.2. Zircon oxygen isotopic data

Zircons from the same dated samples were selected for in situ O isotopic analyses. Generally, the U-Pb age and O isotopic analyses were done on the same sites as shown in Fig. 9. In situ O isotopes for a total of 136 zircon grains were analyzed. The data are listed in Appendix Table 2 and shown in Fig. 11.

Twenty-nine oxygen isotopic spot analyses were obtained for sample Hjbs01-37. The monzogranite yields the $\delta^{18}\text{O}$ values, ranging from $5.2\text{\textperthousand}$ to $6.5\text{\textperthousand}$ with an average value at $5.9\text{\textperthousand}$. Thirty-four spots on the zircon grains from monzogranite (YZHS02-21) at YZHS deposit yield oxygen isotopic compositions of $\delta^{18}\text{O} = 9.0\text{--}10.8\text{\textperthousand}$. Fifty-two spots on zircon grains from K-feldspar granite (GQ01-21, GQ02-17) at GQ deposit yield oxygen isotopic compositions of $\delta^{18}\text{O} = 7.2\text{--}12.0\text{\textperthousand}$. Twenty-one zircons separated from K-feldspar granite (YS03-11) at YS deposit have $\delta^{18}\text{O}$ values ranging from $5.9\text{\textperthousand}$ to $7.8\text{\textperthousand}$ (average = $7.0\text{\textperthousand}$).

5.3. Major and trace element compositions

The granitic samples hosting the orebodies of the Hjbs, YZHS and GQ have similar characteristics. They exhibit high SiO_2 ($73.47\text{--}78.25\text{ wt\%}$), Al_2O_3 ($12.22\text{--}14.42\text{ wt\%}$) and $\text{K}_2\text{O} + \text{Na}_2\text{O}$ ($6.85\text{--}8.35\text{ wt\%}$) contents, but show relatively low CaO ($0.22\text{--}1.32\text{ wt\%}$), MgO ($0.22\text{--}0.44\text{ wt\%}$), TiO_2 ($0.12\text{--}0.24\text{ wt\%}$) and P_2O_5 ($0.02\text{--}0.09\text{ wt\%}$). The high A/CNK values (1.17–1.38) suggest the intrusions to be peraluminous series (Fig. 12a), with the AR values (2.48–3.87) further constraint them to be calc-alkaline rocks (Fig. 12b).

Chondrite-normalized rare earth element (REE) patterns for the Hjbs, GQ and YZHS samples are typical of a “gull” shape, showing a clear enrichment in LREE relative to the HREE ($(\text{La/Yb})_{\text{N}} = 5.98\text{--}10.85$, $4.04\text{--}6.63$ and $5.79\text{--}7.33$ respectively) (Fig. 13a). The Hjbs samples show slightly depletion in Eu ($\text{Eu/Eu}^* = 0.53\text{--}0.80$) while the GQ and YZHS intrusions exhibit stronger negative Eu anomalies ($\text{Eu/Eu}^* = 0.16\text{--}0.34$ and $0.27\text{--}0.55$), which may be attributed to the fractionation of plagioclase. The intrusions are characterized by pronounced negative Nb, Ta, Ti, Zr, Sr and P anomalies and

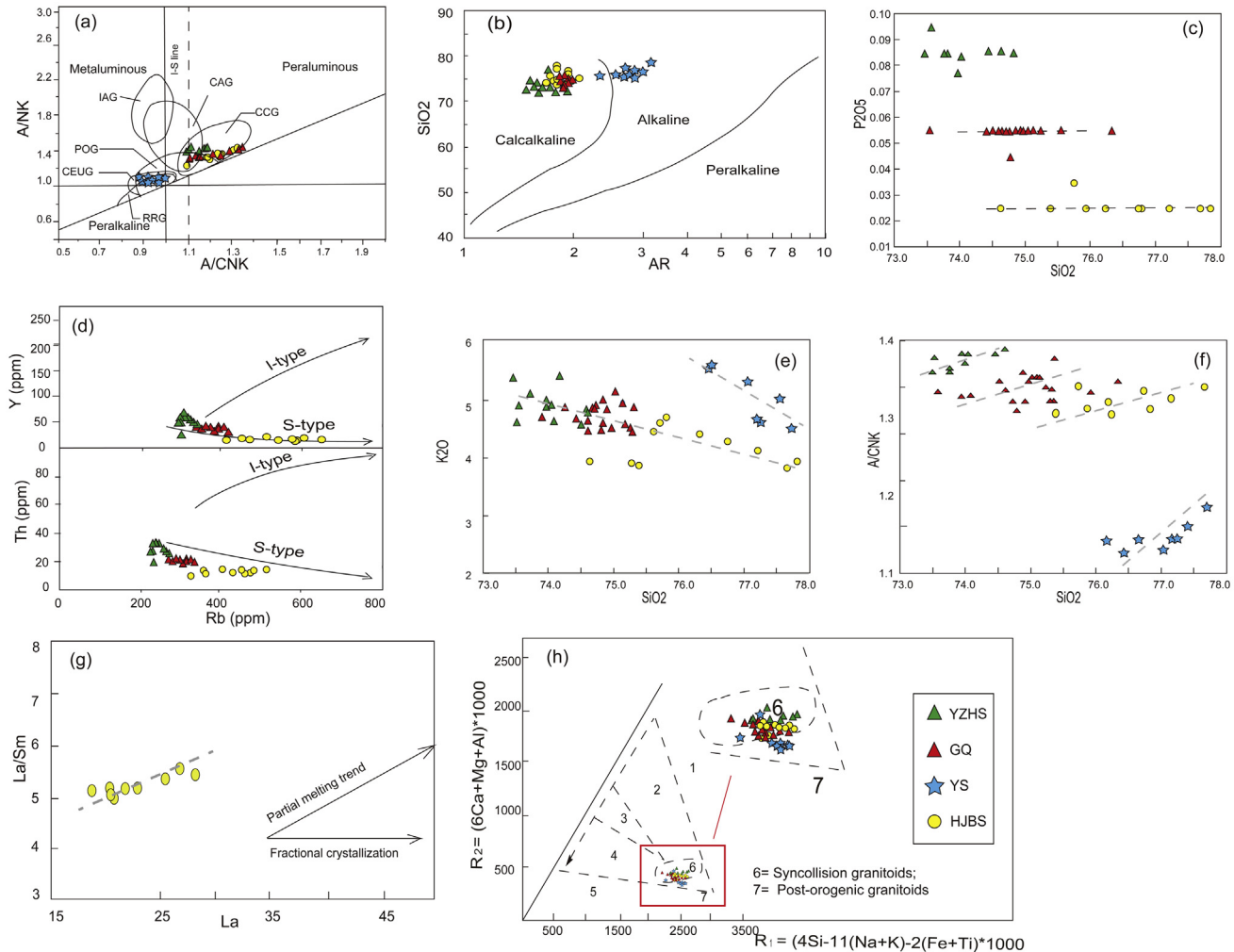


Fig. 12. (a) A/NK vs. A/CNK plot for intrusions from the typical tungsten deposits in Beishan. A/CNK = $\text{Al}_2\text{O}_3/(\text{CaO} + \text{Na}_2\text{O} + \text{K}_2\text{O})$ molar, A/NK = $\text{Al}_2\text{O}_3/(\text{Na}_2\text{O} + \text{K}_2\text{O})$ molar (Maniar and Piccoli, 1989; Peccerillo and Taylor, 1976; Zu et al., 2016). IAG = Island arc granitoids, CAG = continental arc granitoids, CCG = continental collision granitoids, POG = post-orogenic granitoids, RRG = rift-related granitoids, CEUG = continental epeirogenic uplift granitoids; (b) SiO₂ vs. AR diagram, AR = $(\text{Al}_2\text{O}_3 + \text{CaO} + \text{Na}_2\text{O} + \text{K}_2\text{O})/(\text{Al}_2\text{O}_3 + \text{CaO} - \text{Na}_2\text{O} - \text{K}_2\text{O})$ (all weight percent) (Wright, 1969); (c) Plot of P₂O₅ vs. SiO₂; (d) Plots of Y and Th vs. Rb; (e) plot of K₂O and (f) A/CNK vs. SiO₂; (g) La/Sm vs. La diagram; (f) R₂ vs. R₁ diagram, 6 and 7 area represent for the syncollision and post-orogenic granitoids, respectively.

positive Rb, Th, U, Pb and Hf spikes in the primitive mantle normalized spider diagrams (Fig. 13b). The REE and trace element patterns are similar to those of the Silurian arc-related intrusions from the Huaniushan arc and coeval volcanic rocks (Fig. 13a, b).

The YS samples exhibit distinct geochemical characteristics. They have higher SiO₂ (76.16–77.71 wt%), K₂O + Na₂O (8.13–8.80 wt%), FeO/MgO (3.00–5.08), and lower Al₂O₃ (11.71–12.68 wt%), MgO (0.10–0.20 wt%), CaO (0.62–1.57 wt%) and P₂O₅ (~0.01 wt%) (Appendix Table 3). The A/CNK values vary from 0.94 to 1.04, indicating a metaluminous composition (Fig. 12a). The calculated AR value varies between 4.16–5.33 and fall within the range of the alkaline granitoids on a AR vs. SiO₂ discrimination plot (Fig. 12b).

The REE and trace element patterns for YS granites are similar to that of the Triassic A-type granites in Huaniushan deposit in the region (Fig. 13c, d) (Zhu et al., 2012). The $\sum\text{REE}$ ranges from 114 to 206 ppm (Appendix Table 3). The REE patterns are characterized by “tetrad effects”, showing “M” type with scarce LREE/HREE fractionation ($(\text{La}/\text{Yb})_N = 1.93–3.98$) and clear negative Eu anomalies ($\text{Eu}/\text{Eu}^* = 0.10–0.21$) (Fig. 13c). The granite is relatively depleted in Nb, P, Ba, Ti, Zr and Eu, and enriched in large ion lithophile elements (LILE) such as Rb, and Pb (Fig. 13d). Low Ba and Sr

and high Rb and strong negative Eu anomalies are probably attributed to fractional crystallization of plagioclase and orthoclase, whereas depletion in P and Ti might suggest apatite and Ti-rich minerals fractionation.

5.4. Sr and Nd isotopes

The Sr-Nd isotopic data for the samples are listed in Appendix Table 4 and shown in a plot of $\varepsilon\text{Nd}_{(t)}$ versus $(^{87}\text{Sr}/^{86}\text{Sr})_{\text{i}}$ diagram in Fig. 14. Initial Sr isotopic ratio $(^{87}\text{Sr}/^{86}\text{Sr})_{\text{i}}$ values and $\varepsilon\text{Nd}_{(t)}$ values for the Hjbs, GQ, YZHS and YS samples have been calculated at 321.2 Ma, 422.4 Ma, 424.0 Ma and 286.0 Ma respectively based on U-Pb dating on zircons for both suites of rocks. Depleted-mantle model ages ($T_{2\text{DM}}$) are reported using the two-stage model of Liew and Hofmann (1988).

The GQ, YZHS and YS samples show high $(^{87}\text{Sr}/^{86}\text{Sr})_{\text{i}}$ values of 0.7112 to 0.7184. The calculated $\varepsilon\text{Nd}_{(t)}$ values vary from −4.3 to −7.0 with a corresponding $T_{2\text{DM}}$ ages of 1.36–1.73 Ga. The Hjbs samples display calculated initial $(^{87}\text{Sr}/^{86}\text{Sr})_{\text{i}}$ ratios from 0.7029 to 0.7038. The $\varepsilon\text{Nd}_{(t)}$ values for the monzogranites range from 5.9 to 8.3, with $T_{2\text{DM}}$ varying between 404 and 415 Ma.

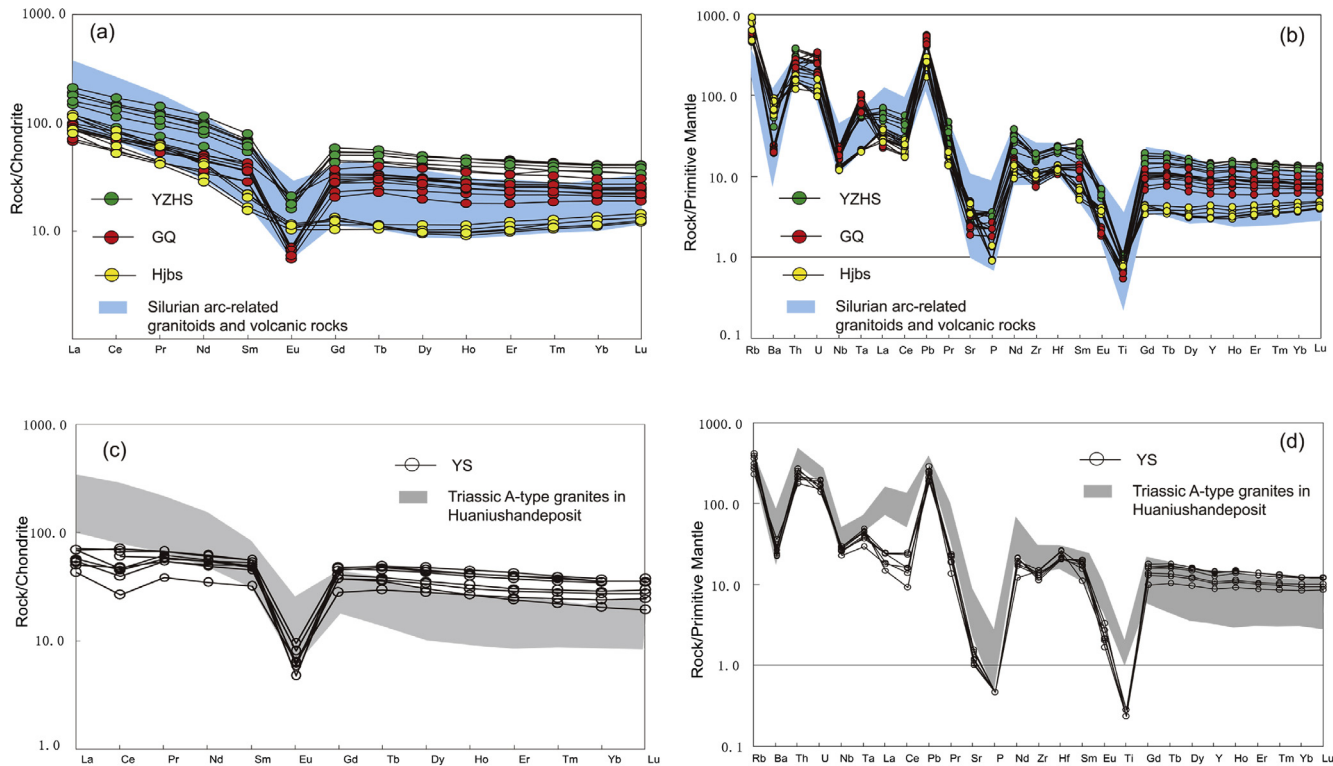


Fig. 13. (a) Chondrite-normalized REE patterns for the Hjbs, GQ and YZHS granite samples. (b) Primitive mantle-normalized spiderdiagrams for the Hjbs, GQ and YZHS granite samples. (c) Chondrite-normalized REE patterns for the YS granite samples. (d) Primitive mantle-normalized spiderdiagrams for the YS granite samples. The chondrite and primitive mantle values are from Sun and McDonough (1989). Values of the Silurian arc-related intrusions and volcanic rocks are from Mao (2008), Li (2011b) and Zhao et al. (2007). Values for the Triassic intrusions in Huanishan tungsten deposit are from Zhu et al. (2012).

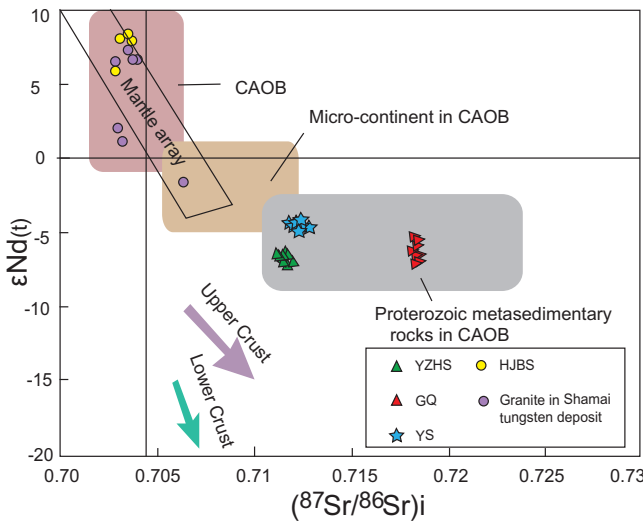


Fig. 14. Diagram of Nd and Sr isotopic variation for the Hjbs, GQ, YZHS and YS granite samples. Basement data for CAOB and microcontinent in CAOB are cited from Hong et al. (2000); Proterozoic metasedimentary rocks are summarized from Yang et al. (2008a), Hu et al. (2000), Gao et al. (2016) and Kröner et al. (2017); granite at the Shamai tungsten deposit in CAOB from Jiang et al. (2016).

6. Discussion

6.1. Petrogenesis and source of the granite

6.1.1. The Hjbs, GQ and YZHS intrusion

The high A/CNK values (1.17–1.38) and generally the presence of aluminous primary minerals such as muscovite and tourmaline

(Fig. 5a-d) in the Hjbs, GQ and YZHS granites, together with the 1.09–3.78% CIPW normative corundum indicate that they are peraluminous and of S-type (Chappell, 1999; Chappell and White, 1992), showing calc-alkaline series nature (Fig. 12a, b). The P_2O_5 contents do not change much with the SiO_2 (Fig. 12c), with Th and Y displaying a negative correlation with Rb (Fig. 12d), also indicating S-type affinities (Green and Watson, 1982; Chappell, 1999; Li et al., 2007), which might source from the crustal sediment. This deduction is further supported by the high SiO_2 and alkalis, low TiO_2 , MgO and CaO contents as well as the high $\text{K}_2\text{O}/\text{Na}_2\text{O}$ (1.02–2.03) ratios and low $\text{Mg}^{\#}$ ($\text{Mg}^{\#} = 100 \times \text{molar Mg}/(\text{Mg} + \text{Fe})$; 11–31) values, which are all indicators of the crust-sourced granitoids (Barbarin, 1999; Li et al., 2015; Mi et al., 2015). The strong depletion of Sr and Ba, and the anomalous high Rb/Sr (2.93–9.21) values, also suggest that the magma originated from partial melting of the continental crust. Hence, the granites were sourced from a continental crust, even though the crust is isotopically young juvenile or old recycled.

The very high initial $^{87}\text{Sr}/^{86}\text{Sr}$ ratios (0.7112–0.7184) and negative $\varepsilon_{\text{Nd}}(t)$ values (-5.6 to -7.0) for GQ and YZHS intrusion with a corresponding $T_{2\text{DM}}$ ages of 1.62 to 1.73 Ga suggest the magma was generated by partial melting of the ancient crust, with the Nd isotope compositions plotting on the evolution field of the Proterozoic crust in CAOB (Fig. 14), suggesting they were sourced from Precambrian metasedimentary strata. The $\delta^{18}\text{O}$ values of 7.2‰ to 12.0‰ further indicate an important contribution of continental crust, which are basically close to the normal $\delta^{18}\text{O}$ range of the terrestrial S-type granites (Valley, 2003; O'Neil and Chappell, 1977). This interpretation is convincingly demonstrated by the low values of δEu (0.16–0.55) and $(\text{La/Yb})_{\text{N}}$ (4.04–7.33), which are characteristic of plagioclase-residual partial melting (Taylor and McLennan, 1985; Mi et al., 2015). Song et al. (2014) have found the granitic

pluton in Huaniushan arc is surrounded by Precambrian metasedimentary rocks. They suggested the granite could have been formed by partial melting of these ancient materials. This appears to be supported by the presented isotopic data.

However, the $\delta^{18}\text{O}$ values (average at 5.9‰) for Hjbs granites are close to the mantle derived igneous zircon (5.3 ± 0.3‰) (Valley et al., 2005). On the $\varepsilon\text{Nd}_{(t)}$ vs. $(^{87}\text{Sr}/^{86}\text{Sr})_i$ diagram (Fig. 14), the samples display positive $\varepsilon\text{Nd}_{(t)}$ (5.9–8.3) values and low $(^{87}\text{Sr}/^{86}\text{Sr})_i$ ratios (0.7029–0.7038), with young $T_{2\text{DM}}$ ages ranging from 404 to 415 Ma. They plot in the CAOB field, similar to granites at Shamai tungsten deposit in CAOB (Fig. 14) (Jiang et al., 2016). Many Phanerozoic granites in the CAOB are characterized by low initial Sr isotopic ratios, positive $\varepsilon\text{Nd}_{(t)}$ values and young Sm-Nd model ages ($T_{2\text{DM}}$) (Hong et al., 2000), indicating their juvenile character and suggesting derivation from source rocks or magma separated shortly from the upper mantle (Jahn et al., 2000; Han et al., 1997; Shen et al., 2017). There exist three possible models for their genesis: (1) granitic liquids generated by interaction of basaltic magma with juvenile crust (Jahn et al., 2000); (2) fractional crystallization of regional mantle-derived mafic parental magma (Han et al., 1997); (3) partial melting of the mafic to intermediate crust (Wu et al., 2003, 2005). However, the lack of coeval mafic volcanic complexes in the region (Fig. 4) excludes the possibility of the former two processes with the low Mg# values (23–27) indicating they were derived by partial melting of a basaltic lower crust rather than a mantle (Rapp and Watson, 1995). Moreover, the marked negative Nb anomalies and positive Pb anomalies on a multi-element normalized spidergram (Fig. 13b) is consistent with the involvement of crustal compositions (Rudnick and Fountain, 1995). On the plots of La/Sm vs. La (Fig. 12g), the samples exhibit a well-defined linear trend,

suggesting that a partial melting process plays an important role in their generation. Pronounced depletions of Ba, Sr, Nb, P, and Ti (Fig. 13b) show that the parental magma has undergone advanced fractional crystallization. Partial melting of juvenile lower crust and subsequent fractional crystallization and assimilation is therefore proposed as a plausible mechanism for the generation of the Hjbs intrusion in the Hanshan terrane.

6.1.2. The YS intrusion

Geochemically, the YS granites display typical characteristics of A-type granite. They have high ratios of $\text{FeO}_T/(\text{FeO}_T + \text{MgO})$ (0.77–0.85, Fig. 15a) and $10,000 \times \text{Ga}/\text{Al}$, high abundances of SiO_2 , $\text{Na}_2\text{O} + \text{K}_2\text{O}$, but low Al_2O_3 , MgO , CaO , TiO_2 and P_2O_5 contents. Additionally, characteristic depletion in Ba, Sr, Ti and enrichment in Th, La, Nd and Ce with pronounced Eu negative anomalies are found in the granites, both are consistent with that for A-type affinity (Collins et al., 1982; Whalen et al., 1987). The mineral compositions are consistent with the aluminous A-type granite, which occur as a suite containing compositional trends with fractional crystallization (Fig. 5e, f). However, the compositions of A-type granites modified by fractional crystallization would tend to be similar to those of highly fractionated S- and I-type granites (Chappell and White, 1992; King et al., 1997). The low abundances of Zr, $(\text{Zr} + \text{Nb} + \text{Ce} + \text{Y})$ and $\sum\text{REE}$ in the YS granites display I-type affinities. Similar characteristics have already been found in aluminous A-type granites in other region (King et al., 1997; Qiu et al., 2004; Dahlquist et al., 2014). Fractional crystallization of minerals which host for Zr and REEs (e.g. zircon and allanite) would be responsible for the decreasing Zr, $(\text{Zr} + \text{Nb} + \text{Ce} + \text{Y})$ and $\sum\text{REE}$ concentrations in both A- and I-type granite (Dahlquist et al., 2014). The $10,000 \times \text{Ga}/\text{Al}$ ratios for the studied rocks vary from 2.70 to

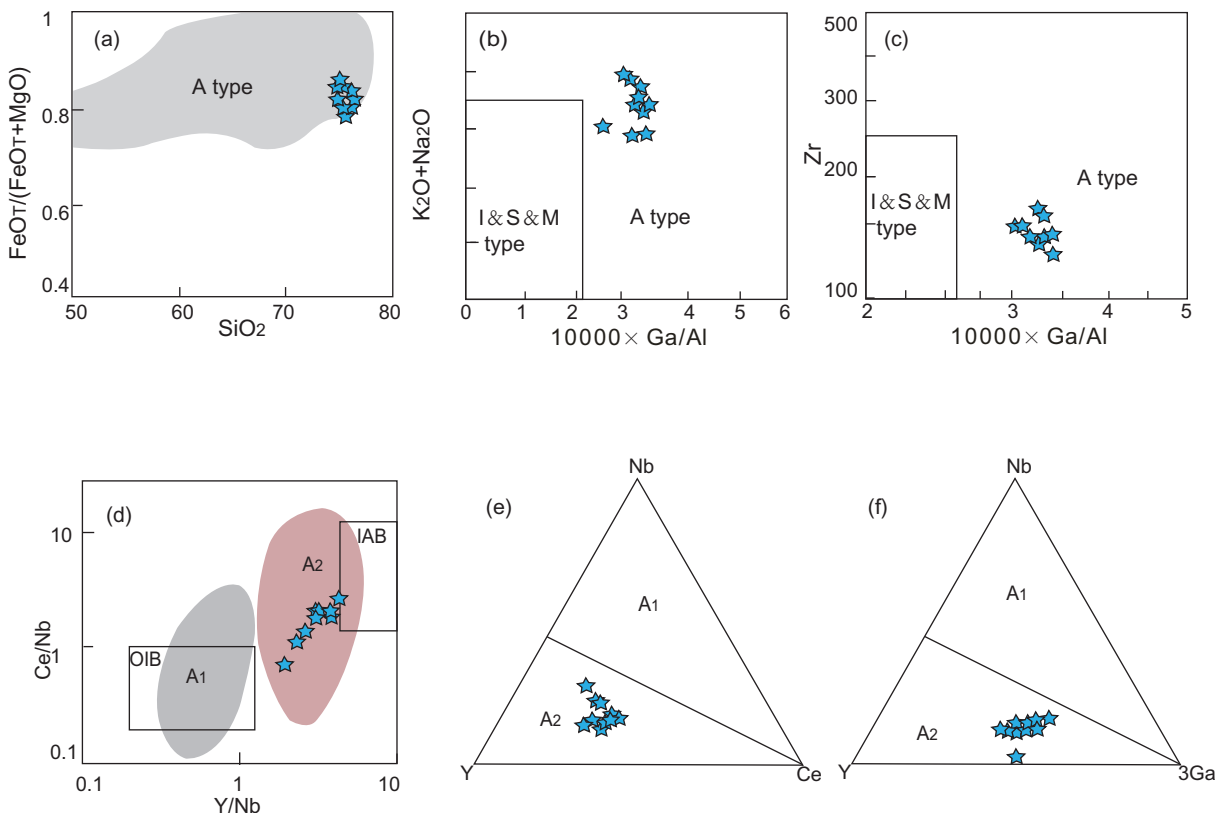


Fig. 15. (a) $\text{FeO}_T/(\text{FeO}_T + \text{MgO})$ vs. SiO_2 ; (b) $\text{Na}_2\text{O} + \text{K}_2\text{O}$ and (c) Zr vs. $10,000 \times \text{Ga}/\text{Al}$ (Whalen et al., 1987), showing the A-type signature of the YS granites; The A-type granite subdivision diagrams of (d) Ce/Nb vs. Y/Nb , (e) $\text{Nb}-\text{Y}-\text{Ce}$ and (f) $\text{Nb}-\text{Y}-3\text{Ga}$ (Eby, 1992), showing the YS granites belong to the A₂ subgroup, A₁ = intracontinental rift or mantle plume background, A₂ = regional post-orogenic extension background, symbols as in Fig. 12.

3.45, average at 3.15, higher than those of I- and S-type granites (2.10 and 2.28 respectively) and similar to the global average of 2.6 for A-type granites (Whalen et al., 1987). Besides, the YS granites have extremely low P_2O_5 (~0.01 wt%), low A/CNK (0.94–1.04) and high Na_2O contents (3.25–4.53 wt%) obviously different from the fractionated S-type granites (Chappell, 1999; King et al., 1997). Hence, the YS granites are highly evolved aluminous A-type granites instead of highly fractionated I- or S-type granites. On the discriminant diagrams of $(K_2O + Na_2O)$ and Zr vs. $10,000 \times Ga/Al$ (Fig. 15b, c), the studied granites are plotted in the A-type granite field. The high Ce/Nb and Y/Nb ratios indicate that they belong to the A₂-type granites (Fig. 15d) (Eby, 1992), consistent with that shown in the triangle diagram of Nb-Y-Ce and Nb-Y-3Ga (Fig. 15e, f).

It has been stated that the A₂ group represents magmas derived from continental crust or underplated crust that has been through a cycle of continent-continent collision or island-arc magmatism (Collins et al., 1982; Whalen et al., 1987; Eby, 1992; Frost et al., 2002). Compared with the suggested ratios of Ce/Pb and Nb/U for primitive mantle (9 and 30) and continental crust (4 and 10) (Hofmann et al., 1986), The Ce/Pb (average at 3) and Nb/U ratios (average at 6) for the YS A-type granite imply that it was substantially derived from crust. The YS K-feldspar granites have $\delta^{18}O$ values ranging from 5.9‰ to 7.8‰, suggesting a crustal derivation (Valley, 2003; O'Neil and Chappell, 1977). The fairly consistent negative $\varepsilon_{Nd(t)}$ (−4.3 to −4.8), with relatively high initial $^{87}Sr/^{86}Sr$ ratios (0.7120 to 0.7128) plus the two-stage model ages of 1.36 to 1.47 Ga, would further support the interpretation that they were mainly generated from Precambrian metasedimentary materials (Fig. 14) (Yang et al., 2008a).

6.2. Magma evolution and tungsten mineralization

The studied Hjbs, YZHS, GQ and YS granite mainly crop out in the respective orefield, detailed field work has shown that the granites and orebodies intercalate with each other (Figs. 4, 6–8), indicating a temporal and spatial link between the magmatism and mineralization.

Tungsten is a highly incompatible element. It has been continuously enriched towards the crust during earth evolution, leading to the result that tungsten is concentrated in the crust, especially in the ancient crust rather than the mantle (König et al., 2011; Lehmann, 1994). Furthermore, W abundance in sedimentary rocks, as well as in related metamorphic rocks is much higher than that in ultramafic, mafic, and intermediate rocks (Liu and Ma, 1987; Chi et al., 2012). The aforementioned variable O and Sr-Nd isotopic compositions in Hjbs, GQ, YZHS and YS granite indicate an origin via the partial melting of the crust (Precambrian metasedimentary strata or juvenile lower crust), which will contribute to the enrichment of tungsten element. Partial melting in the presence of favorable complex agents can also lead to additional enrichment of tungsten (Liu et al., 2015).

Additionally, most granites associated with W mineralization are highly fractionated (Huang and Jiang, 2014; Jiang et al., 2016; Neiva, 2002). Fractional crystallization is a very important mechanism that could further enrich W-Sn in magma (Fogliata et al., 2012; Huang and Jiang, 2014; Teixeira et al., 2012). The very high Rb and pronounced low Ba, Sr, Nb, P, Eu and Ti concentrations indicate that highly fractional crystallization has been involved in the generation of the Hjbs, GQ, YS and YZHS granite (Fig. 13b, d). The significant negative Eu, Ba and Sr anomalies indicate that feldspar is present as a residual phase, and negative P anomaly should have resulted from apatite fractionation. To achieve the pronounced Eu depletion (Fig. 13a, c), a large quantity of plagioclase fractionation is required. The negative correlation between SiO_2 and K_2O

(Fig. 12e) is also ascribed to the feldspar fractional crystallization. Nb and Ta have affinity to Ti and are commonly hosted in Ti-bearing oxides (e.g. ilmenite, rutile and titanite) and silicates (e.g., biotite and amphibole) (Tiepolo et al., 2000; Xiong et al., 2011; Stepanov et al., 2014). The depletion in Ti, Nb and Ta has been commonly attributed to fractionation of ilmenite, biotite and/or rutile. The fractional crystallization would conduce to W-Sn enrichment in the magma.

Alternatively, high concentrations of W in the granites may be also controlled by magmatic-hydrothermal processes. The granitic samples exhibit a REE 'tetrad effect' (Fig. 13a, c), which is the typical signature of highly evolved melts and has been generally attributed to fractional crystallization during granite differentiation (McLennan, 1994) or to interaction of granitic melts with hydrothermal fluids (Irber, 1999; Monecke et al., 2002). The highly evolved magmatic system is rich in volatile phase (e.g. H_2O , CO_2) and elements such as W, Sn, Li, B, F, or Cl, while the hydrothermal fluids in these deposits have been substantiated to be mainly evolved from a magmatic origin. Consequently, abundant volatile phase and rare-metal minerals (tungsten included) were retained in the fluid-melt system, which will contribute to the formation of an economically important ore deposit. Furthermore, fluid inclusions found in the quartz phenocrysts from the granites without visible alteration indicate that the evolved melts underwent volatile phase exsolution after fractional crystallization, providing a more favorable condition for the extraction of W from the magma. Fluid/melt partition coefficients of W increase with increasing melt peraluminosity (Zajacz et al., 2008), while differentiation of the magma, as demonstrated by the positive correlation between A/CNK and SiO_2 (Fig. 12f), is supposed to lead the residual melt to become more and more peraluminous and to undergo volatile phase exsolution, and finally lead the W mineralization. The granites associated with mineralization at Hjbs, GQ, YZHS and YS were crystallized during a long time interval. This indicates that there is a long period of fractional crystallization and magmatic-hydrothermal history which was favorable to W mineralization as large voluminous W-bearing fluids could be extracted after the magma experienced intense fractionation over a prolonged period. In other words, the highly fractionated magma and the prolonged magmatic-hydrothermal interaction jointly contributed to the formation of the W deposit.

6.3. Geochronological framework

The time of the tungsten deposits and associated intrusions is poorly constrained, and most geochronological data are whole-rock K-Ar, Ar-Ar and Sm-Nd ages, with few Re-Os and Rb-Sr ages (Nie et al., 2002a, 2002b, 2002c, 2003, 2004; Li and Chen, 2004; Li et al., 2005), which provide limited constraints on the timing of the magmatism and mineralization, because the granitic samples were exposed to the magmatic hydrothermal alteration and may have gone through the process of greisenization, tourmalinization and silicification. Recently, the intrusions have been dated by SHRIMP U-Pb, LA-ICPMS U-Pb, TIMS U-Pb and SIMS U-Pb methods on zircons as well (Li et al., 2011; Yang et al., 2008a,b, 2010; Zhao et al., 2010, 2011, 2012; Zhang et al., 2008c; Ma and Xi, 2012).

Yang et al. (2008b) obtained a K-Ar isochron age of 370 Ma for the quartz diorite and 375 Ma for the biotite granite from the Baixianishan tungsten deposit. They also obtained TIMS U-Pb zircon ages of 379.7 to 405.4 Ma and 380 Ma for the quartz diorite and biotite granite respectively (Table 2). Li et al. (2011) suggested the rock and ore-forming age of GQ ore-hosting intrusion is 439.1 ± 8.0 Ma while Yang et al. (2010) got a LA-ICPMS zircon U-Pb age of 392.0 ± 55.0 Ma, and we obtained new SIMS U-Pb zircon ages of 422.4 ± 4.8 Ma and 416.9 ± 7.1 Ma for the GQ intrusion

Table 2

Summary of isotopic dating of mineralization and associated rocks.

Location	Deposit	Rock-types	Fraction	Ages (Ma)	Dating methods	Reference
XHT	Liushashan	Molybdenite	Molybdenite	260 ± 10	Re-Os	Nie et al. (2003)
XHT	Liushashan	Quartz diorite	Whole rock	262 ± 4	K-Ar	Nie et al. (2002b)
XHT	Liushashan	Quartz diorite	Whole rock	261 ± 3	K-Ar	Nie et al. (2002b)
XHT	Hjbs	Monzogranite	Apatite	322.0 ± 3.9	Sm-Nd	Nie et al. (2004)
XHT	Hjbs	Monzogranite	Zircon	314.2 ± 2.4	LA-ICPMS U-Pb	Yang et al. (2008a,b)
XHT	Hjbs	Monzogranite	Zircon	321.2 ± 2.7	SIMS U-Pb	This article
XHT	Xiaobaishitou	Ore	Scheelite	244 ± 5	Rb-Sr	Li and Chen (2004)
XHT	Xiaobaishitou	Biotite adamellite	Quartz	248 ± 7	Rb-Sr	Li et al. (2005)
SHA	Baixianishan	QUARTZ diorite	Zircon	379.7–405.4	TIMS U-Pb	Yang et al. (2008a)
SHA	Baixianishan	Quartz diorite	Whole rock	370	K-Ar	Yang et al. (2008a)
SHA	Baixianishan	Biotite granite	Zircon	380	U-Pb	Yang et al. (2008a)
SHA	Baixianishan	Biotite granite	Whole rock	375	K-Ar	Yang et al. (2008a)
SHA	GQ	K-feldspar granite	Zircon	392.0 ± 55.0	LA-ICPMS U-Pb	Yang et al. (2010)
SHA	GQ	K-feldspar granite	Zircon	439.1 ± 8.0	LA-ICPMS U-Pb	Li et al. (2011)
SHA	GQ	K-feldspar granite	Zircon	422.4 ± 4.8	SIMS U-Pb	This article
SHA	GQ	K-feldspar granite	Zircon	416.9 ± 7.1	SIMS U-Pb	This article
SHA	YZHS	Monzogranite	Zircon	398.9 ± 2.9	LA-ICPMS U-Pb	Yang et al. (2008a)
SHA	YZHS	Monzogranite	Whole rock	361.9	K-Ar	Yang et al. (2010)
SHA	YZHS	Monzogranite	Zircon	424.0 ± 3.2	SIMS U-Pb	This article
SHA	YS	K-feldspar granite	Zircon	272.0	TIMS U-Pb	Nie et al. (2002a)
SHA	YS	K-feldspar granite	Zircon	285.0 ± 5.0	SHRIMP U-Pb	Zhang et al. (2008c)
SHA	YS	K-feldspar granite	Zircon	286.0 ± 4.1	SIMS U-Pb	This article

Note: XHT = Xingxingxia-Hanshan Terrane; SHA = Shuangyingshan-Huaniushan Arc.

(Table 2). Yang et al. (2010) carried out a K-Ar dating on the monzogranite of YZHS deposit and obtained an isochron age of 361.9 Ma, they also got a LA-ICPMS zircon U-Pb age of 398.9 ± 2.9 Ma (Yang et al., 2008b) and we obtained a new SIMS U-Pb zircon age of 424.0 ± 3.2 Ma for the YZHS monzogranite (Table 2), which was slightly younger than the Gongpoquan Cu deposit of 426.0 ± 2.8 Ma (Ding, unpublished data). Nie et al. (2004) proposed a Sm-Nd isochron age of 322.0 ± 3.9 Ma for the Hjbs monzogranite while Yang et al. (2008a, 2008b) reported the monzogranite was emplaced at 314.2 ± 2.4 Ma, and we obtained a SIMS zircon U-Pb age of 321.2 ± 2.7 Ma for the Hjbs ore-hosting intrusion (Table 2). In summary, these isotopic data suggest that the rock-forming and mineralization ages of the deposits range between lower Silurian and lower Carboniferous (424–314 Ma).

Nie et al. (2002b, 2003) suggested that the rock- and ore-forming ages of the Liushashan tungsten deposit are 261 ± 3–262 ± 4 Ma and 260 ± 10 Ma, respectively (Table 2). Li and Chen (2004) and Li et al. (2005) used Rb-Sr methods to determine the ages of quartz and scheelite from the Xiaobaishitou ore-bearing rocks and obtained ages of 248 ± 7 and 244 ± 5 million years, respectively (Table 2). Nie et al. (2002a) got a TIMS zircon U-Pb age of 272.0 Ma for an ore-bearing moyite in the YS deposit (Table 2). We obtained a new SIMS U-Pb zircon ages of 286.0 ± 4.1 Ma for the intrusion, close to the previously reported SHRIMP zircon U-Pb age of 285.0 ± 5.0 Ma from Zhang et al. (2008c), and is slightly older than the Baishantang Cu deposit of 274.3 ± 1.6 Ma (Ding, unpublished data) in the same region. These isotopic data indicate that the rock- and ore-forming events of the deposits occurred in the Permian (286–244 Ma).

Based on our analysis and published ages (Table 2), and combining this study with the late Paleozoic intrusions and associated mineralization (Table 1), two episodes of magmatism related to coeval tungsten mineralization have been recognized in the BOB, as exemplified by the Hjbs, GQ, YZHS and Baixianishan deposit for the 424–314 Ma system and by Xiaobaishitou, Liushashan and YS deposit for the 286–244 Ma one. These two magmatic events are well recorded throughout the Shuangyingshan-Huaniushan arc and Hanshan block, both represented by scattered intrusions.

6.4. Tectonic model for the granites and tungsten mineralization

The 424–314 Ma Hjbs, GQ and YZHS granite exhibit negative Eu anomalies and are characterized by enrichments in Rb, Th, U and Hf and depletions in high field strength elements (HFSE) such as Nb, Ta, Ti, Zr, P and HREE (Fig. 13a, b), which are consistent with normal arc magma (Richards, 2003; Sillitoe, 2010). They plot in the continental collision field in the A/NK-A/CNK diagram (Fig. 12a) and in syncollision field in the R_1 vs. R_2 diagram (Fig. 12h) (Batchelor and Bowden, 1985). Therefore, the intrusions were speculated to have formed in an arc-collision setting. During the Ordovician to the Early Silurian time, the intervening oceans between blocks were subducted to the margin of pre-existing ancient Hanshan and Shuangyingshan continental blocks (Fig. 16a), forming the Queershan, Hanshan, Gongpoquan and Shuangyingshan-Huaniushan arcs (Fig. 16b). However, the Hanshan and Gongpoquan arcs amalgamated to each other in the Middle Silurian, marking the development of the early stage of the Gongpoquan arc-accretionary system (Phase I, Fig. 16c) while the system accreted to the Shuangyingshan-Huaniushan arc in the Late Silurian to Early Devonian time to form the middle stage of the arc-accretionary system (Phase II, Fig. 16d). The arc-collision has triggered the remelting of pre-existing ancient materials in Shuangyingshan-Huaniushan arc and lead to the voluminous W-rich granitic magmatism and related mineralization (eg. GQ, YZHS and Baixianishan) (Fig. 16d), which is consistent with the negative $\varepsilon_{Nd(t)}$, high ($^{87}Sr/^{86}Sr$)_i and old T_{2DM} values. By the Middle Devonian time, an intraoceanic Heiyingshan arc was generated by north-dipping subduction between the arc-accretionary system and the Queershan arc (Fig. 16d), which aggregated with the arc-accretionary system in the Middle to Late Carboniferous to form the mature stage of Gongpoquan arc-accretionary system (Phase III, Fig. 16e). The convergence might have resulted in remelting of juvenile lower crust in Hanshan arc and promote the magmatism and mineralization at Hjbs, supported by the positive $\varepsilon_{Nd(t)}$ values and young T_{2DM} ages. In general, the subduction-accretion and arc amalgamations between the Siberia and Dunhuang block resulted in the development of Gongpoquan arc-accretionary system and related granitic magmatism and tungsten deposits during Silurian to Carboniferous (Fig. 16).

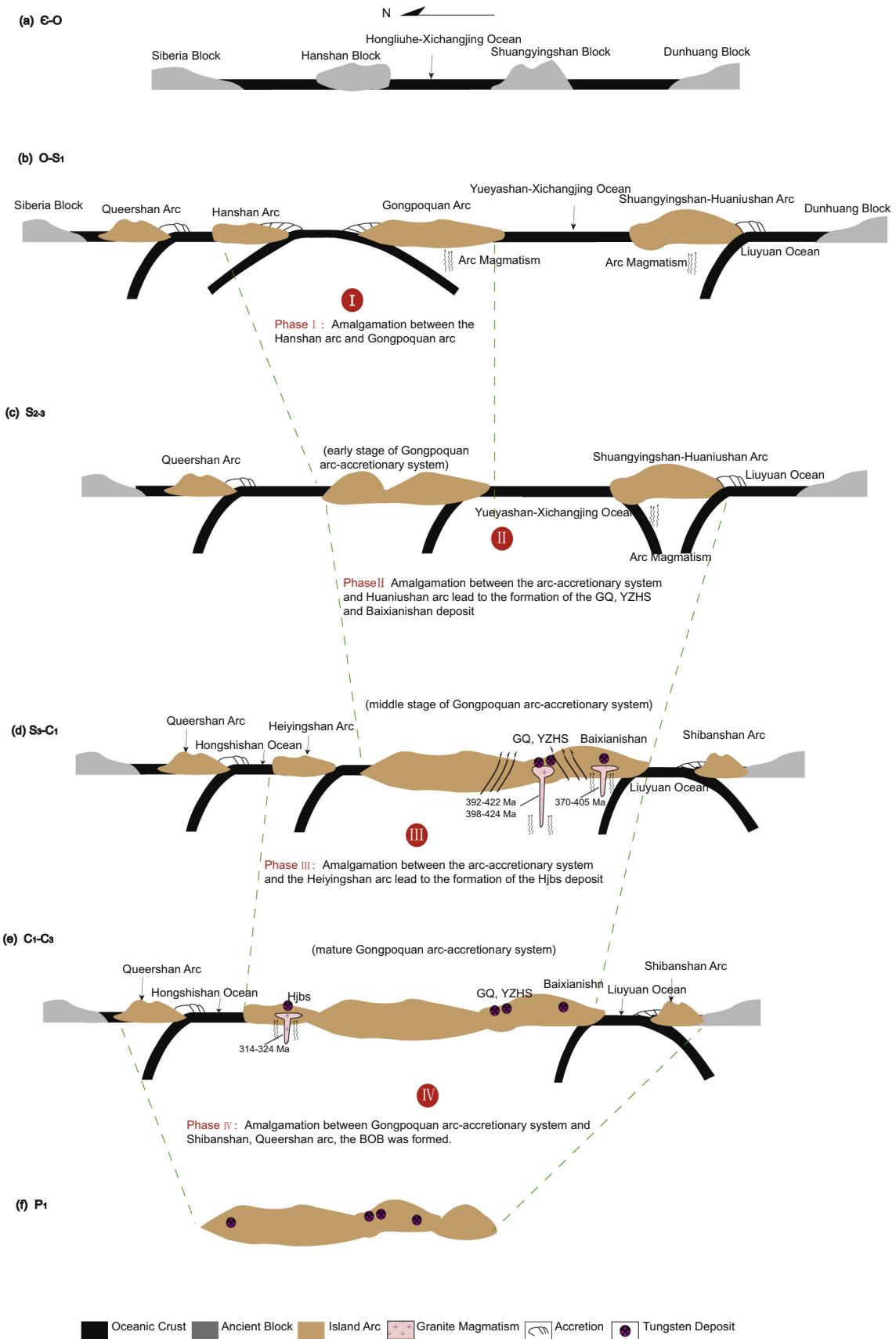


Fig. 16. Sequential diagram illustrating the Paleozoic tectonic evolution of Beishan Orogenic Belt and initiation of Silurian to Carboniferous arc accretion-related tungsten deposits (based on our own work and modified after Xiao et al., 2010).

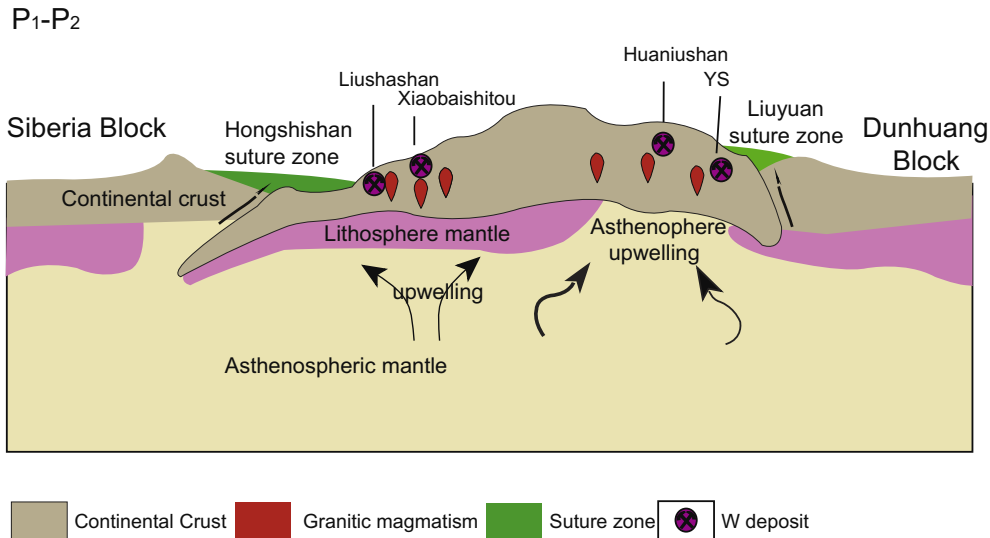


Fig. 17. Speculative geodynamic model of Beishan Orogenic Belt during Permian time and the associated tungsten deposits.

However, the Permian zoned YS granite is considered to be A₂-type affinity (Fig. 15), indicating a post-orogenic extension environment on a local or regional scale (Fig. 12a, h) (Whalen et al., 1987; Eby, 1992; Zhang et al., 2008a,b, 2012a). Paleomagnetic, geochronology and stratigraphic data show that the archipelago convergence and syn-collisional crust shortening had ended at the end of Carboniferous to Permian time, the subsequent post-collisional extension began (Tian et al., 2014) (Fig. 16f, phase IV, Fig. 17). It was proved by the widespread post-collisional mafic-ultramafic rocks and A-type granitic stocks throughout the area (Li et al., 2011; Zhu et al., 2012; Pirajno et al., 2009; Wu et al., 2011; in press). The ages of granitic magmatism range from 290 to 220 Ma (Li et al., 2011). The post-collisional extension stage is supposed to be responsible for the widespread emplacement of 286–244 Ma granites and associated contemporaneous W-(Mo) deposits (e.g. the YS, Huaniushan, Xiaobaishitou and Liushashan deposit) (Fig. 17).

The BOB is the southernmost segment of the Altaids, which extends eastwards through the East Tien Shan suture to the Solonker suture (Fig. 1) and occupies a key position to the CAOB (Zheng et al., 2014). It has been previously recognized that the BOB was produced by multiple accretion and amalgamations of island arcs from the Cambrian to Permian as a result of prolonged subduction and closure of branches of Paleoasian Ocean between the Dunhuang Block and Siberia Craton (Figs. 16 and 17) (Windley et al., 2007; Ao et al., 2010; Xiao et al., 2010; Song et al., 2013a). Based on the tectonic evolution, geochemical and geochronological data, we recognized two distinctive metallogenetic models related to tungsten mineralization in the BOB, i.e. the arc-accretion mineralization system formed at 424–314 Ma and the post-collision system at 286–244 Ma.

7. Conclusions

Based on a combined in situ zircon U-Pb, O and Sr-Nd isotopic study of late Palaeozoic intrusions in the BOB, we draw the following conclusions.

- (1) Two major suites of intrusions associated with tungsten mineralization have been recognized during 424–314 Ma (Suite I) and 286–244 Ma (Suite II) in the BOB.

- (2) The whole rock Sr-Nd and zircon O isotopic compositions indicate that the intrusions of Suite I were derived from the partial melting of Precambrian metasedimentary strata (GQ, YZHS) or juvenile lower crust (Hjbs), whereas Suite II was derived from the ancient crustal sediment (YS).
- (3) The geochemical features of the granites show a prolonged magmatic-hydrothermal interaction to be responsible for the tungsten mineralization, and the tungsten mineralization was found to be closely related to the emplacement of the highly fractionated granites.
- (4) The Silurian to Carboniferous tungsten deposits in the BOB were closely associated with the arc-collision, supporting an arc-accretion system model is considered to be the best explanation while the Permian mineralization is related to a post-collision event.

Conflict of interest

We declare that we have no financial and personal relationships with other people or organizations that can appropriately influence our work, there is no professional or other personal interest of any nature or kind in any product, service and/or company that could be construed as influencing the position presented in, or the review of, the manuscript entitled.

Funding

This work was supported by the National Natural Science Foundation Projects [41121890] and the National 305 Projects [2011BAB06B04-1].

Acknowledgements

We are grateful to He Li and Xiao-Mei Yang for their help with elemental analyses and to Prof. Xian-Hua Li and Dr. Xiao-Yan Jiang for assisting with the zircon U-Pb and O isotopic analyses. We are grateful to Prof. Jiyuan Yin, Dr. Yinzhaoh Wang, Bo Zu, Xiujin Liu, Chang Zhang and Qingfeng Mei for helpful discussions and assistances during the revision of this paper. Prof. Taofa Zhou and two anonymous reviewers are thanked for their constructive and detailed review of this manuscript.

Appendix A. Supplementary data

Supplementary data associated with this article can be found, in the online version, at <http://dx.doi.org/10.1016/j.oregeorev.2017.06.018>.

References

- Ao, S.J., Xiao, W.J., Han, C.M., Li, X.H., Qu, J.F., Zhang, J.E., Guo, Q.Q., Tian, Z.H., 2012. Cambrian to early Silurian ophiolite and accretionary processes in the Beishan collage, NW China: implications for the architecture of the Southern Altaiids. *Geol. Mag.* 149, 606–625.
- Barbarin, B., 1999. A review of the relationships between granitoid types, their origins and their geodynamic environments. *Lithos* 46, 605–626.
- Batchelor, R.A., Bowden, P., 1985. Petrogenetic interpretation of granitoid rock series using multication parameters. *Chem. GeoL* 48, 43–55.
- Chappell, B.W., 1999. Aluminium saturation in I- and S-type granites and the characterization offractionation hapogranoites. *Lithos* 46, 535–551.
- Chappell, B.W., White, A.J.R., 1992. I- and S-type granites in the Lachlan Fold Belt. *Trans. Royal Soc. Edinburgh Earth Sci.* 83, 1–26.
- Chen, Y.R., 2006. Geological characteristics and genetic analysis of Xiaobaishitou W-Mo deposit. *Xinjiang Gansu Metall.* 28, 612–618 (in Chinese with English abstract).
- Cheng, J., Zhang, D.Z., 2012. Discussion on ore-forming conditions of Baishantang copper deposit. *Gansu Metall.* 34, 73–77.
- Chi, Q.H., Wang, X.Q., Xu, S.F., Zhou, J., Liu, H.L., Liu, D.S., Zhang, B.M., Wang, W., 2012. Temporal and spatial distribution of tungsten and tin in South China Continent. *Earth Sci. Front.* 19, 70–83 (in Chinese with English abstract).
- Collins, W.J., Beams, S.D., White, A.J.R., Chappell, B.W., 1982. Nature and origin of A-type granites with particular reference to Southeastern Australia. *Contrib. Miner. Petrol.* 80, 189–200.
- Dahlquist, J.A., Alasino, P.H., Bello, C., 2014. Devonian F-rich peraluminous A-type magmatism in the proto-Andean foreland (Sierras Pampeanas, Argentina): geochemical constraints and petrogenesis from the western-central region of the Achala batholith. *Mineral. Petrol.* 108, 391–417.
- Dai, W.J., 2010. Geochemical features and geological significance of mafic and ultra-mafic rock in Sidingheishan of Beishan region, Gansu province. *Gansu Geol.* 19, 8–17 (in Chinese with English abstract).
- Ding, J.X., Han, C.M., Xiao, W.J., Wang, Z.M., Yang, X.M., 2015. Geochemistry and U-Pb geochronology of tungsten deposit of Huanushan island arc in the Beishan Orogenic Belt, and its geodynamic background. *Acta Petrol. Sin.* 31, 594–616 (in Chinese with English abstract).
- Eby, G.N., 1992. Chemical subdivision of the A-type granitoids: petrogenetic and tectonic implications. *Geology* 20, 641–644.
- Fogliati, A.S., Báez, M.A., Hagemann, S.G., Santos, J.O., Sardi, F., 2012. Post-orogenic, Carboniferous granite-hosted Sn-W mineralization in the Sierras Pampeanas Orogen, Northwestern Argentina. *Ore Geol. Rev.* 45, 16–32.
- Frost, C.D., Frost, B.R., Bell, J.M., Chamberlain, K.R., 2002. The relationship between A-type granites and residual magmas from anorthosite: evidence from the northern Sherman batholith, Laramie Mountains, Wyoming, USA. *Precambr. Res.* 119, 45–71.
- Gao, S., Liu, X.M., Yuan, H.L., Hattendorf, B., Günther, D., Chen, L., Hu, S.H., 2002. Determination of forty two major and trace elements in USGS and NIST SRM glasses by laser ablation inductively coupled plasma-mass spectrometry. *Geostand. Newslett.* 26, 191–196.
- Gao, X.F., Guo, F., Xiao, P.X., Kang, L., Xi, R.G., 2016. Geochemical and Sr-Nd-Pb isotopic evidence for ancient lower continental crust beneath the Xi ujimugui area of NE China. *Lithos* (in press).
- Green, T.H., Watson, E.B., 1982. Crystallization of apatite in natural magmas under high pressure, hydrous conditions, with particular reference to orogenic rock series. *Contrib. Mineral. Petrol.* 79, 96–105.
- Guo, Q.Q., Xiao, W.J., Windley, B.F., Mao, Q.G., Han, C.M., Qu, J.F., Ao, S.J., Li, J.L., Song, D.F., Yong, Y., 2012. Provenance and tectonic settings of Permian turbidites from the Beishan Mountains, NW China: implications for the Late Paleozoic accretionary tectonics of the southern Altaiids. *J. Asian Earth Sci.* 49, 54–68.
- Han, B.F., Wang, S.G., Jahn, B.M., Hong, D.W., Kagami, H., Sun, Y.L., 1997. Depleted-mantle source for the Ulungur River A-type granites from North Xinjiang, China: geochemistry and Nd-Sr isotopic evidence, and implications for Phanerozoic crustal growth. *Chem. Geol.* 138, 135–159.
- Han, C.M., Xiao, W.J., Zhao, G.C., Mao, J.W., Li, S.Z., Yan, Z., Mao, Q.G., 2016. Major types, characteristics and geodynamic mechanism of Upper Paleozoic copper deposits in northern Xinjiang, northwestern China. *Ore Geol. Rev.* 28, 308–328.
- He, Z.Z., 2015. Geological characteristics and prospecting of Saozishan Au deposit, Gansu. *Gansu Sci. Technol.* 31, 20–24 (in Chinese with English abstract).
- He, Z.Z., Dong, Q.W., 2012. Geological characteristics and prospecting of Huanangou W-Mo deposit, Gansu. *Gansu Sci. Technol.* 14, 32–34 (in Chinese with English abstract).
- Hofmann, A.W., Jochum, K.P., Seufert, M., White, W.M., 1986. Nb and Pb in oceanic basalts: new constraints on mantle evolution. *Earth Planet. Sci. Lett.* 79, 33–45.
- Hong, D.W., Wang, S.G., Xie, X.L., Zhang, J.S., 2000. Genesis of positive $\epsilon_{Nd(t)}$ granitoids in the Da Hinggan Mts. Mongolia orogenic belt and growth continental crust. *Earth Sci. Front.* 7, 441–456 (in Chinese with English abstract).
- Hoskin, P.W.O., Black, L.P., 2000. Metamorphic zircon formation by solid-state recrystallization of protolith igneous zircon. *J. Metamorph. Geol.* 18, 423–439.
- Hu, P., 2007. *Tectonomagmatic Evolution and Gold Metallogeny in South Beishan Mountain, Northwest China*. Chinese Academy of Geological Sciences, Beijing, pp. 1–155 (in Chinese with English abstract, Ph.D. thesis).
- Hu, A.Q., Wang, Z.G., Tu, G.Z., 1996. *Geological Evolution and Diagenetic Mineralization Regularity of Northern Xinjiang*. Science Press, Beijing, pp. 1–246 (in Chinese with English abstract).
- Hu, A.Q., Jahn, B.M., Zhang, G.X., Chen, Y.B., Zhang, Q.F., 2000. Crustal evolution and Phanerozoic crustal growth in northern Xinjiang: Nd isotopic evidence. Part I. Isotopic characterization of basement rocks. *Tectonophysics* 328, 15–51.
- Huang, L.C., Jiang, S.Y., 2014. Highly fractionated S-type granites from the giant Dahutang tungsten deposit in Jiangnan Orogen, Southeast China: geochronology, petrogenesis and their relationship with W-mineralization. *Lithos* 202–203, 207–226.
- Hui, W.D., Zhu, J., Deng, J., Lv, X.B., Mo, Y.L., Li, C.C., 2013. U-Pb geochronology and geochemical characteristics of rhyolitic porphyry in the Baishantang mine, Beishan, Gansu and their geological implications. *Geol. Explor.* 49, 484–495 (in Chinese with English abstract).
- Irber, W., 1999. The lanthanide tetrad effect and its correlation with K/Rb, Eu/Eu*, Sr/Eu, Y/Ho, and Zr/Hf of evolving peraluminous granite suites. *Geochim. Cosmochim. Acta* 63, 489–508.
- Jahn, B.M., Wu, F.Y., Chen, B., 2000. Massive granitoid generation in central Asia: Nd isotopic evidence and implication for continental growth in the Phanerozoic. *Episodes* 23, 82–92.
- Jahn, B.M., Windley, B.F., Natal'in, B., Dobretsov, N., 2004. Phanerozoic continental growth in Central Asia. *J. Asian Earth Sci.* 23, 599–603.
- Jiang, S.H., 2004. *Magmatism and Gold Metallogeny in Beishan Mt., Northwestern China*. Chinese Academy of Geological Sciences, Beijing, pp. 1–179 (in Chinese with English abstract, Ph.D. thesis).
- Jiang, S.H., Nie, F.J., 2006. ^{40}Ar - ^{39}Ar geochronology of Hongjianbingshan tungsten deposit in Beishan mountain, Gansu province, China. *Min. Depos.* 25, 89–94 (in Chinese with English abstract).
- Jiang, S.H., Nie, F.J., Hu, P., Lai, X.R., 2006. Discussion on the relationship of magmatism and gold metallogeny in Beishan mountain area. *Min. Depos.* 25, 269–272 (in Chinese with English abstract).
- Jiang, S.H., Leon, B., Hu, P., Han, N., Chen, L.C., Liu, Y., Kang, H., 2016. Zircon U-Pb ages and Sr-Nd-Hf isotopes of the highly fractionated granite with tetrad REE patterns in the Shamal tungsten deposit in eastern Inner Mongolia, China: implications for the timing of mineralization and ore genesis. *Lithos* 261, 322–339.
- King, P.L., White, A.J.R., Chappell, W., Allen, C.M., 1997. Characterization and origin of aluminous A-type granites from the Lachlan Fold Belt, Southeastern Australia. *J. Petrol.* 38, 371–391.
- König, S., Münker, C., Hohl, S., Paulick, H., Barth, A.R., Lagos, M., Pfänder, J., Büchl, A., 2011. The Earth's tungsten budget during mantle melting and crust formation. *Geochim. Cosmochim. Acta* 75, 2119–2136.
- Kröner, A., Alexieiev, D.V., Kovach, V.P., Rojas-Agramonte, Y., Tretyakov, A.A., Mikolajchuk, A.V., Xie, H., Sobel, E.R., 2017. Zircon ages, geochemistry and Nd isotopic systematics for the Palaeoproterozoic 2.3–1.8 Ga Kuilyu Complex, East Kyrgyzstan–The oldest continental basement fragment in the Tianshan orogenic belt. *J. Asian Earth Sci.* 135, 122–135.
- Lehmann, B., 1994. Granite-related rare metal mineralization: a general geochemical framework. *Czech Geol. Survey* 21, 324–349.
- Li, P., 2011a. *Geological Characteristics and Genesis of Hongjianbingshan Tungsten Deposit, Beishan MT, Gansu Prov. China University of Geosciences, Wuhan*, pp. 1–127 (in Chinese with English abstract, Master thesis).
- Li, S., 2011b. Definition of Early Mesozoic Granitoids From Beishan Orogen, Origin and Their Tectonic Significance, and Spatio-Temporal Distribution of Early Mesozoic Granitoids in Central and South CAOB. Chinese Academy of Geological Sciences, Beijing, pp. 1–114 (in Chinese with English abstract, Ph.D. thesis).
- Li, H.Q., Chen, F.W., 2004. *Isotope Geochronology of Regional Mineralization in Xinjiang, NW China*. Geological Publishing House, Beijing, pp. 1–391 (in Chinese).
- Li, H.Q., Wu, H., Chen, F.W., Deng, G., Yang, H.M., Yang, Z.F., Mei, Y.P., Guo, J., 2005. New chronological evidence for Indosian diagenetic mineralization in eastern Xinjiang, NW China. *Acta Geol. Sin.* 79, 264–275 (in Chinese with English abstract).
- Li, X.H., Li, W.X., Li, Z.X., 2007. On the genetic classification and tectonic implications of the Early Yanshanian granitoids in the Nanling Range, South China. *Chin. Sci. Bull.* 52, 1873–1885.
- Li, X.H., Liu, Y., Li, Q.L., Guo, C.H., Chamberlain, K.R., 2009. Precise determination of Phanerozoic zircon Pb/Pb age by multi-collector SIMS without external standardization. *Geochim. Geophys. Geosyst.* 10, Q04010. <http://dx.doi.org/10.1029/2009GC002400>.
- Li, X.H., Li, W.X., Li, Q.L., Wang, X.C., Liu, Y., Yang, Y.H., 2010a. Petrogenesis and tectonic significance of the ~850 Ma Gangbian alkaline complex in South China: evidence from in situ zircon U-Pb dating, Hf-O isotopes and whole-rock geochemistry. *Lithos* 114, 1–15.
- Li, X.H., Long, W.G., Li, Q.L., 2010b. Penglai zircon megacrysts: a potential new working reference material for microbeam determination of Hf-O isotopes and U-Pb age. *Geostand. Geoanal. Res.* 34, 117–134.
- Li, P., Lv, X.B., Chen, C., Cao, X.F., Mayila, A., Su, Y.Y., 2011. Chronology and geochemical characteristics of K-feldspar granite in the Guoqing tungsten deposit and their geological implications. *Acta Petrol. Mineral.* 30, 13–24 (in Chinese with English abstract).

- Li, N., Chen, Y.J., Santosh, M., Pirajno, F., 2015. Compositional polarity of Triassic granitoids in the Qinling Orogen, China: implication for termination of the northernmost paleo-Tethys. *Gondwana Res.* 27, 244–257.
- Liew, T.C., Hofmann, A.W., 1988. Precambrian crustal components, plutonic associations, plate environment of the Hercynian Fold Belt of central Europe: indications from a Nd and Sr isotopic study. *Contrib. Mineral. Petrol.* 98, 129–138.
- Liu, Y.J., Ma, D.S., 1987. *Geochemistry of Tungsten*. Science Press, Beijing (in Chinese).
- Liu, Y., Nie, F.J., Jiang, S.H., 2001. The copper-bearing porphyries of Elegenwulanwula deposit, Inner Mongolia. *Min. Depos.* 20, 199 (in Chinese with English abstract).
- Liu, D.X., Dong, Y.Q., Zhang, Y.B., 2009. Characteristics of mineralization of Nanjinshan-Langwashan gold metallogenic belt in Beishan Area, Gansu Province. *Gansu Geol.* 18, 29–33 (in Chinese with English abstract).
- Liu, X., Xing, H., Zhang, D., 2015. The mechanisms of the infill textures and its implications for the five-floor zonation at the Dajishan vein-type tungsten deposit, China. *Ore Geol. Rev.* 65, 365–374.
- Liu, Y.G., Lv, X.B., Wu, C.M., Hu, X.G., Duan, Z.P., Deng, G., Wang, H., Zhu, X.K., Zeng, H.D., Wang, P., Wang, W., Lu, Q., 2016. The migration of Tarim plume magma toward the northeast in Early Permian and its significance for the exploration of PGE-Cu-Ni magmatic sulfide deposits in Xinjiang, NW China: as suggested by Sr-Nd-Hf isotopes, sedimentology and geophysical data. *Ore Geol. Rev.* 72, 538–545.
- Ludwig, K.R., 2003. User's Manual for Isoplot 3.00: A Geochronological Toolkit for Microsoft Excel. Berkeley Geochronol. Center Spec. Publ. 4, 1–70.
- Lv, B., Yang, Y.Q., Meng, G.X., Yan, J.Y., Zhao, J.H., Wang, S.G., Jia, L.L., Peng, R.M., 2011. Geochemical characteristics and petrogenesis of Dongqiyishan alkali feldspar granite, Inner Mongolia. *Acta Petrol. Mineral.* 30, 543–552 (in Chinese with English abstract).
- Ma, D.C., Xi, Z., 2012. The ore-controlling factors of Yushan tungsten deposit. *Northwestern Geol.* 45, 57–60 (in Chinese).
- Maniar, P.D., Piccoli, P.M., 1989. Tectonic discrimination of granitoids. *Geol. Soc. Am. Bull.* 101, 635–643.
- Mao, Q.G., 2008. Paleozoic to Early Mesozoic Accretionary and Collisional Tectonics of the Beishan and Adjacent Area, Northwest China. Institute of Geology and Geophysics, Chinese Academy of Sciences, Beijing, China, pp. 1–228 (in Chinese with English abstract, Ph.D. thesis).
- McLennan, S.M., 1994. Rare-earth element geochemistry and the tetrad effect. *Geochim. Cosmochim. Acta* 58, 2025–2033.
- Mi, M., Chen, Y.J., Yang, Y.F., Wang, P., Li, F.L., Wan, S.Q., Xu, Y.L., 2015. Geochronology and geochemistry of the giant Qian'echong Mo deposit, Dabie Shan, eastern China: implications for ore genesis and tectonic setting. *Gondwana Res.* 27, 1217–1235.
- Monecke, T., Kempf, U., Monecke, J., Sala, M., Wolf, D., 2002. Tetrad effect in rare earth element distribution patterns: a method of quantification with application to rock and mineral samples from granite-related rare metal deposits. *Geochim. Cosmochim. Acta* 66, 1185–1196.
- Nasdala, L., Hofmeister, W., Norberg, N., Mattinson, J.M., Corfu, F., Dörr, W., Kamo, S. L., Kennedy, A.K., Kröner, A., Reiners, P.W., Frei, D., Kosler, J., Wan, Y., Götz, J., Häger, T., Kröner, A., Valley, J.W., 2008. Zircon M257—a homogeneous natural reference material for the ion microprobe U-Pb analysis of zircon. *Geostand. Geoanal. Res.* 32, 247–265.
- Neiva, A.M.R., 2002. Portuguese granites associated with Sn-W and Au mineralizations. *Bull. Geol. Soc. Finland* 74, 79–101.
- Nie, F.J., Jiang, S.H., Bai, D.M., 2002a. Metallogenetic Studies and Ore Prospecting in the Conjunction Area of Inner Mongolia Autonomous Region, Gansu Province and Xinjiang Uyghur Autonomous Region (Beishan Mt.), Northwest China. Geological Publishing House, Beijing, pp. 1–480 (in Chinese).
- Nie, F.J., Jiang, S.H., Zhao, S.M., Bai, D.M., Liu, Y., Zhao, Y.M., Wang, X.L., Su, X.X., 2002b. Geological characteristics and types of Liushashan Au (Mo) deposit, Inner Mongolia. *Geol. Geochem.* 30, 1–7 (in Chinese with English abstract).
- Nie, F.J., Jiang, S.H., Zhao, X.M., Bai, D.M., Li, Q.Z., Guo, X.D., 2002c. Geological features and origin of the Zhaoibishan gold deposit in Beishan Region, Northwest China. *Chin. J. Geol.* 37, 207–218 (in Chinese with English abstract).
- Nie, F.J., Jiang, S.H., Bai, D.M., Zhang, Y., Zhao, Y.M., Wang, X.L., 2003. Type and temporal-spatial distribution of metal deposits in the Beishan Mountains, Inner Mongolia and its Neighboring Region. *Acta Geol. Sin.* 77, 367–378 (in Chinese with English abstract).
- Nie, F.J., Jiang, S.H., Hu, P., Zhang, Y., 2004. Geological features and ore-forming material sources of Hongjianbingshan tungsten deposit in Beishan mountain, Gansu province. *Min. Depos.* 23, 11–19 (in Chinese with English abstract).
- O'Neil, J.R.O., Chappell, B.W.J., 1977. Oxygen and hydrogen isotope relations in the Berridale batholith. *J. Geol. Soc. London* 133, 559–571.
- Peccerillo, A., Taylor, S.R., 1976. Geochemistry of Eocene calcalkaline volcanic rocks from the Kastamou area, Northern Turkey. *Contrib. Miner. Petrol.* 58, 63–81.
- Peng, Z.A., Li, H.H., Qu, W.J., Zhang, S.Q., Ding, H.J., Chen, X.R., Zhang, B., Zhang, Y.Z., Xu, M., Cai, M.H., 2010. Molybdenite Re-Os age of Xiaohulishan molybdenum deposit in Beishan area, Inner Mongolia. *Min. Geol.* 29, 510–516.
- Pirajno, F., Ernst, R.E., Borisenco, A.S., Fedoseev, G., Naumov, E., 2009. Intraplate magmatism in Central Asia and China and associated metallogeny. *Ore Geol. Rev.* 35, 114–136.
- Qiu, J.S., Wang, D.Z., McInnes, B.I.A., Jiang, S.Y., Wang, R.C., Kanisawa, S., 2004. Two subgroups of A-type granites in the coastal area of Zhejiang and Fujian Provinces, SE China: age and geochemical constraints on their petrogenesis. *Trans. R. Soc. Edinburgh Earth Sci.* 95, 227–236.
- Rapp, R.P., Watson, E.B., 1995. Dehydration melting of metabasalt at 8–32 kbar: implications for continental growth and crust-mantle recycling. *J. Petrol.* 36, 891–931.
- Richards, J.P., 2003. Tectono-magmatic precursors for porphyry Cu-(Mo-Au) deposit formation. *Econ. Geol.* 98, 1515–1533.
- Rudnick, R.L., Fountain, D.M., 1995. Nature and composition of the continental crust—a lower crustal perspective. *Rev. Geophys.* 33, 267–309.
- Sengör, A.M.C., Natalin, B.A., Buttman, U.S., 1993. Evolution of the Altaiid tectonic collage and Paleozoic crustal growth in Eurasia. *Nature* 364, 299–307.
- Shen, P., Pan, H.D., Cao, C., Zhong, S.H., Li, C.H., 2017. The formation of the Suyunhe large porphyry Mo deposit in the West Junggar terrain, NW China: zircon U-Pb age, geochemistry and Sr-Nd-Hf isotopic results. *Ore Geol. Rev.* 81, 808–828.
- Sillitoe, R.H., 2010. Porphyry copper systems. *Econ. Geol.* 105, 3–41.
- Sláma, J., Košler, J., Condon, D.J., Crowley, J.L., Gerdes, A., Hanchar, J.M., Horstwood, M.S.A., Morris, G.A., Nasdala, L., Norberg, N., Schaltegger, U., Schoene, B., Tubrett, M.N., Whitehouse, M.J., 2008. Plešovice zircon—a new natural reference material for U-Pb and Hf isotopic microanalysis. *Chem. Geol.* 249, 1–35.
- Song, D.F., Xiao, W.J., Han, C.M., Li, J.L., Qu, J.F., Guo, Q.Q., Lin, L.N., Wang, Z.M., 2013a. Progressive accretionary tectonics of the Beishan orogenic collage, southern Altaids: insights from zircon U-Pb and Hf isotopic data of high-grade complexes. *Precambrian Res.* 227, 368–388.
- Song, D.F., Xiao, W.J., Han, C.M., Tian, Z.H., Wang, Z.M., 2013b. Provenance of metasedimentary rocks from the Beishan orogenic collage, southern Altaids: constraints from detrital zircon U-Pb and Hf isotopic data. *Gondwana Res.* 24, 1127–1151.
- Song, D.F., Xiao, W.J., Han, C.M., Tian, Z.H., 2014. Geochronological and geochemical study of gneiss-schist complexes and associated granitoids, Beishan Orogen, southern Altaids. *Int. Geol. Rev.* 55, 1705–1727.
- Stacey, J.S., Kramers, J.D., 1975. Approximation of terrestrial lead isotope evolution by a two-stage model. *Earth Planet. Sci. Lett.* 26, 207–221.
- Stepanov, A., Mavrogenes, J.A., Meffre, S., Davidson, P., 2014. The key role of mica during igneous concentration of tantalum. *Contrib. Miner. Petrol.* 167, 2013–2023.
- Su, B.X., Qin, K.Z., Tang, D.M., Patrick, A.S., Liu, P.P., Sun, H., Xiao, Q.H., 2013. Late Paleozoic mafic-ultramafic intrusions in southern Central Asian Orogenic Belt (NW China): Insight into magmatic Ni-Cu sulfide mineralization in orogenic setting. *Ore Geol. Rev.* 51, 57–73.
- Sun, Y.J., Li, D.M., 2009. Mineralization pattern of Baixianishan tungsten deposit. *Gansu Sci. Technol.* 25, 23–26 (in Chinese with English abstract).
- Sun, S.S., McDonough, W.F., 1989. Chemical and isotopic systematics of oceanic basalts: implications for mantle composition and processes. *Geol. Soc. London Spec. Publ.* 42, 313–345.
- Taylor, S.R., McLennan, S.M., 1985. The Continental Crust: Its Composition and Evolution. Blackwell, Oxford, pp. 1–312.
- Teixeira, R.J.S., Neiva, A.M.R., Gomes, M.E.P., Corfu, F., Cuesta, A., Croudace, I., 2012. The role of fractional crystallization in the genesis of early syn-D3, tin-mineralized Variscan two-mica granites from the Carrazeda de Ansiães area, northern Portugal. *Lithos* 153, 177–191.
- Tian, Z.H., Xiao, W.J., Shan, Y.H., Windley, B., Han, C.M., Zhang, J.E., Song, D.F., 2013. Mega-fold interference patterns in the Beishan orogen (NW China) created by change in plate configuration during Permo-Triassic termination of the Altaids. *J. Struct. Geol.* 52, 119–135.
- Tian, Z.H., Xiao, W.J., Shan, Y.H., Windley, B., Han, C.M., Zhang, J.E., Wan, B., Ao, S.J., Song, D.F., Feng, J.Y., 2014. Structures, ages and tectonic development of the Huoshishan-Niujiuzi ophiolitic mélange, Beishan, southernmost Altaids. *Gondwana Res.* 25, 820–841.
- Tiepolo, M., Vannucci, R., Oberti, R., Foley, S., Bottazzi, P., Zanetti, A., 2000. Nb and Ta incorporation and fractionation in titanian pargasite and kaersutite: crystal-chemical constraints and implications for natural systems. *Earth Planet. Sci. Lett.* 176, 185–201.
- Valley, J.W., 2003. Oxygen Isotopes in Zircon. *Rev. Mineral. Geochem.* 53, 343–385.
- Valley, J.W., Lackey, J.S., Cavosie, A.J., Clechenko, C.C., Spicuzza, M.J., Basei, M.A.S., Bindeman, I.N., Ferreira, V.P., Sial, A.N., King, E.M., Peck, W.H., Sinha, A.K., Wei, C., 2005. 4.4 billion years of crustal maturation: oxygen isotope ratios of magmatic zircon. *Contrib. Miner. Petrol.* 150, 561–580.
- Wang, Q.L., Chen, W., Han, D., Wang, C.Y., Liu, X.Y., Zhang, S.H., 2008. The age and mechanism of formation of the Jinwozi gold deposit, Xinjiang. *Geol. China* 35, 286–292 (in Chinese with English abstract).
- Whalen, J.B., Currie, K.L., Chappell, B.W., 1987. A-type granites: geochemical characteristics, discrimination and petrogenesis. *Contrib. Miner. Petrol.* 95, 401–419.
- Windley, B.F., Alexeev, D., Xiao, W., Kröner, A., Badarch, G., 2007. Tectonic models for accretion of the Central Asian Orogenic Belt. *J. Geol. Soc. London* 164, 31–47.
- Wright, J.B., 1969. A simple alkalinity ratio and its application to questions of non-igneous granite genesis. *Geol. Mag.* 106, 370–384.
- Wu, F.Y., Jahn, B.M., Wilde, S.A., Lo, C.H., Yui, T.F., Lin, Q., Ge, W.C., Sun, D.Y., 2003. Highly fractionated I-type granites in NE China (II): isotopic geochemistry and implications for crustal growth in the Phanerozoic. *Lithos* 67, 191–204.
- Wu, F.Y., Lin, J.Q., Wilde, S.A., Zhang, X.O., Yang, J.H., 2005. Nature and significance of the Early Cretaceous giant igneous event in eastern China. *Earth Planet. Sci. Lett.* 233, 103–119.
- Wu, F.Y., Sun, D.Y., Ge, W.C., Zhang, Y.B., Grant, M.L., Wilde, S.A., Jahn, B.M., 2011. Geochronology of the Phanerozoic granitoids in northeastern China. *J. Asian Earth Sci.* 41, 1–30.

- Xiao, W.J., Kusky, T., 2009. Geodynamic processes and metallogenesis of the Central Asian and related orogenic belt. *Gondwana Res.* 16, 167–169.
- Xiao, W.J., Mao, Q.G., Windley, B.F., Han, C.M., Qu, J.F., Zhang, J.E., Ao, S.J., Guo, Q.Q., Cleven, N.R., Lin, S.F., Shan, Y.H., Li, J.L., 2010. Paleozoic multiple accretionary and collisional processes of the Beishan orogenic collage. *Am. J. Sci.* 310, 1553–1594.
- Xiong, X.L., Keppler, H., Audébat, A., Ni, H.W., Sun, W.D., Li, Y., 2011. Partitioning of Nb and Ta between rutile and felsic melt and the fractionation of Nb/Ta during partial melting of hydrous metabasalt. *Geochim. Cosmochim. Acta* 75, 1673–1692.
- Xu, R.K., Lu, S.Z., Li, X.D., Zheng, Y.Y., Sun, X.C., Wei, Z., Shan, L., Zhang, Y.L., Liu, Y.P., 2010. Metallotectonic anatomy and metallogenic prognosis for ore-concentrated area of Gongpoquan copper deposit from Beishan area of Gansu Province. *Geol. Explor.* 46, 93–101.
- Yang, S.S., 2012. Characteristics of Porphyry-Type Ore Deposits and Ore-Forming System Analysis in North Beishan Area, Inner Mongolia. China University of Geosciences, Beijing, pp. 1–169 (in Chinese with English abstract, Ph.D. thesis).
- Yang, J.H., Chung, S.L., Wilde, S.A., Wu, F.Y., Chu, M.F., Lo, C.H., Fan, H.R., 2006. Petrogenesis of post-orogenic syenites in the Sulu Orogenic Belt, east China: geochronological, geochemical and Nd-Sr isotopic evidence. *Chem. Geol.* 235, 186–190.
- Yang, H.Q., Li, Y., Zhao, G.B., Yang, J.G., Li, W.M., Yang, L.H., 2008a. The Research Results Report on prospecting problems in Beishan metallogenic belt. pp. 1–321 (in Chinese).
- Yang, H.Q., Li, Y., Li, W.M., Yang, J.G., Zhao, G.B., Sun, N.Y., Wang, X.H., Tan, W.J., 2008b. General discussion on metallogenic tectonic setting of Beishan Mountain, northwestern China. *Northwestern Geol.* 41, 22–28 (in Chinese with English abstract).
- Yang, F.Q., Mao, J.W., Bierlein, F.P., Pirajno, F., Zhao, C.S., Ye, H.S., Liu, F., 2009. A review of the geological characteristics and geodynamic mechanisms of Late Paleozoic epithermal gold deposits in North Xinjiang, China. *Ore Geol. Rev.* 35, 217–234.
- Yang, H.Q., Zhao, G.B., Li, W.M., Yang, J.G., Li, Y., Wang, X.H., Jiang, H.B., Tan, W.J., 2010. Formation age and source tracing of the tungsten-bearing granite belt in the Guoqing-Yingzuihongshan area, Inner Mongolia. *Geol. Explor.* 46, 353–370 (in Chinese).
- Yang, S.S., Wang, S.G., Shen, C.L., Zhang, M., Zhang, H.X., Zheng, B.J., Jia, L.L., Zhuang, Y., Zhou, L.J., 2012. Rock-forming and ore-forming age of Xiaohulishan molybdenum-polymetallic deposit in Inner Mongolia and its geological significance. *Geoscience* 26, 261–268.
- Yang, J.G., Wang, L., Xie, X., Wang, X.H., Qi, Q., Jiang, A.D., Zhang, Z.Y., 2016. SHRIMP zircon U-Pb age and its signification of Guashishan mafic-ultramafic complex in Beishan Mountains, Gansu Province. *Geotect. Metall.* 40, 98–108 (in Chinese with English abstract).
- You, X.M., 2002. Study on the Metallogeny of Copper Deposits in Beishan Area, Gansu Province. Zhongnan University, Hunan, pp. 1–43 (in Chinese with English abstract, Ph.D. thesis).
- Zajacz, Z., Halter, W.E., Pettke, T., Guillong, M., 2008. Determination of fluid/melt partition coefficients by LA-ICPMS analysis of co-existing fluid and silicate melt inclusions: controls on element partitioning. *Geochim. Cosmochim. Acta* 72, 2169–2197.
- Zhang, Z.J., Chen, Y.J., Chen, H.Y., Bao, J.X., 2002. Study on the fluid inclusions of Jiwozi gold deposit in Xinjiang. *Min. Depos.* 21, 1099–1101.
- Zhang, Q., Wang, Y., Pan, G.Q., Li, C.D., Jin, W.J., 2008a. Sources of granites: some crucial questions on granite study(4). *Acta Petrol. Sin.* 24, 1193–1204 (in Chinese with English abstract).
- Zhang, Q., Wang, Y.L., Jin, W.J., Jia, X.Q., Li, C.D., 2008b. Criteria for the recognition of pre-, syn- and post-orogenic granitic rocks. *Geol. Bull. China* 27, 1–18 (in Chinese with English abstract).
- Zhang, X.H., Su, L., Cui, X.J., Ding, S.H., Zhao, J.G., Chen, L., 2008c. The Age and Controlling factors of Yushan tungsten deposit, Beishan Orogen, Gansu Province. *Sci. China* 53, 1077–1084 (in Chinese with English abstract).
- Zhang, Q., Ran, B.H., Li, C.D., 2012a. A-type granite: what is the essence? *Acta Petrol. Mineral.* 31, 621–626 (in Chinese with English abstract).
- Zhang, W., Pease, V., Wu, T., Zheng, R., Feng, J., He, Y., Luo, H., Xu, C., 2012b. Discovery of an adakite-like pluton near Dongqiyishan (Beishan, NW China)—its age and tectonic significance. *Lithos* 142–143, 148–160.
- Zhang, S.M., Wang, T.Y., Zhang, H., Zhang, Z.G., Yang, R., Fan, L.X., 2014. Ore-controlling factors and geological features of the W-Sn polymetallic ore deposits in East Qiyi Shan, Inner Mongolia. *Geol. Explor.* 50, 1038–1049 (in Chinese with English abstract).
- Zhao, Z.H., Guo, Z.J., Wang, Y., 2007. Geochronology, geochemical characteristics and tectonic implications of the granitoids from Liuyuan area, Beishan, Gansu province, northwest China. *Acta Petrol. Sin.* 23, 1847–1860.
- Zhao, G.B., Li, W.M., Yang, H.Q., Tian, Y.T., Quan, S.C., Qiao, G.B., Lei, Y.X., Du, T., Gao, Y.W., Yang, T., Feng, B., 2010. Geological and geochemical characteristics of the Guoqing tungsten deposit in Beishan Orogen, Inner Mongolia. *Min. Depos.* 29, 341–342 (in Chinese with English abstract).
- Zhao, G.B., Li, W.M., Yang, H.Q., Tian, Y.T., Gao, Y.W., Du, T., Quan, S.C., Qiao, G.B., Lei, Y.X., Yang, T., Feng, B., 2011. Geological and geochemical characteristics of the Guoqing tungsten-bearing granite mass in Inner Mongolia and its genesis. *Geol. Explor.* 47, 828–836 (in Chinese with English abstract).
- Zhao, G.B., Li, W.M., Yang, H.Q., Gao, Y.W., Yang, T., Jia, J., Quan, S.C., Qiao, G.B., Lei, Y.X., 2012. Mineralization and Prospecting characteristics of the Guoqing tungsten-bearing granite mass in Inner Mongolia. *Northwestern Geol.* 45, 68–71 (in Chinese).
- Zhao, Y., Xue, C.J., Zhao, X.B., Yang, Y.Q., Ke, J.J., Zu, B., Zhang, G.Z., 2016. Origin of anomalously Ni-rich parental magmas and genesis of the Huangshannan Ni-Cu sulfide deposit, Central Asian Orogenic Belt, Northwestern China. *Ore Geol. Rev.* 77, 57–71.
- Zheng, R.G., Wu, T.R., Zhang, W., Meng, Q.P., Zhang, Z.Y., 2014. Geochronology and geochemistry of late Paleozoic magmatic rocks in the Yinwaxia area, Beishan: implications for rift magmatism in the southern Central Asian Orogenic Belt. *J. Asian Earth Sci.* 91, 39–55.
- Zhou, S.M., Sun, B.F., 2015. Genesis analysis of Zhenshifeng tungsten deposit in Gansu Province. *Gansu Sci. Technol.* 31, 30–31 (in Chinese with English abstract).
- Zhu, J., Lv, X.B., Cao, X.F., Mo, Y.L., Chen, C., 2012. U-Pb zircon geochronology, geochemistry and kinetics of the Huaniushan A-type granite in Northwest China. *Chin. J. Geochem.* 31, 85–94.
- Zu, B., Xue, C.J., Chi, G.X., Zhao, X.B., Li, C., Zhao, Y., Yalikun, Y., Zhang, G.Z., Zhao, Y., 2016. Geology, geochronology and geochemistry of granitic intrusions and the related ores at the Hongshan Cu-polymetallic deposit: Insights into the Late Cretaceous post-collisional porphyry-related mineralization systems in the southern Yidun arc, SW China. *Ore Geol. Rev.* 77, 25–42.
- Zuo, G.C., He, G.Q., 1990. Plate Tectonics and Metallogenic Regularities in Beishan Region. Peking University Press, Beijing, pp. 1–226 (in Chinese).
- Zuo, G.C., Zhang, S.L., He, G.Q., Zhang, Y., 1990. Early paleozoic plate tectonics in Beishan area. *Sci. Geol. Sin.* 25, 305–314 (in Chinese with English abstract).
- Zuo, G.C., Liu, Y.K., Liu, C.Y., 2003. Framework and evolution of the tectonic structure in Beishan area across Gansu province, Xinjiang autonomous region and Inner Mongolia autonomous region. *Acta Geol. Gansu* 12, 1–15 (in Chinese).